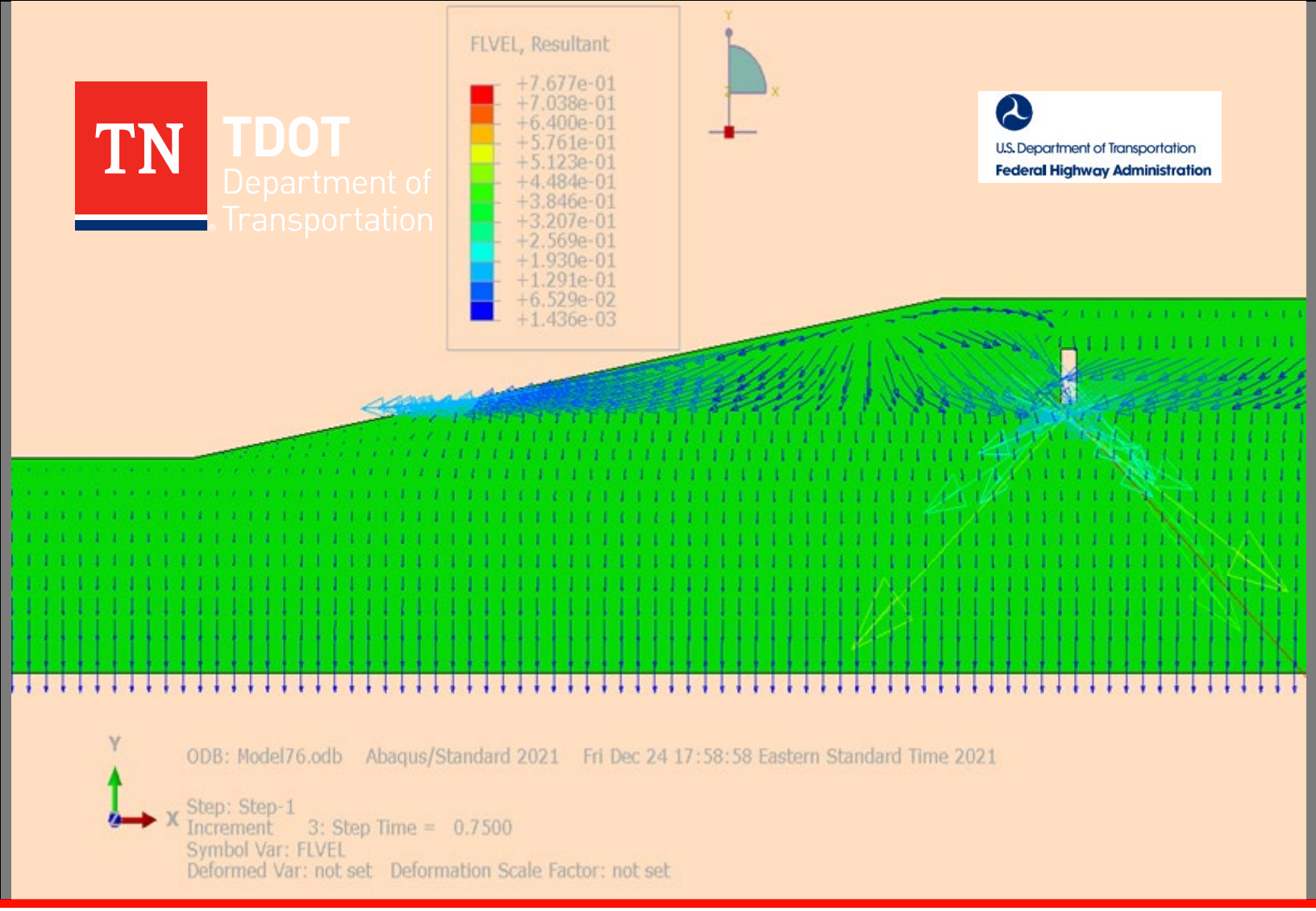

Evaluating Roadway Subsurface Drainage Practices

Research Final Report from the University of Tennessee, Knoxville | Baoshan Huang, Qiang He, Christopher Wilson, Hang Lu, Pawel Polaczyk | May 30, 2022

Sponsored by Tennessee Department of Transportation Long Range Planning Research Office & Federal Highway Administration

THE UNIVERSITY OF TENNESSEE KNOXVILLE

DISCLAIMER

This research was funded through the State Planning and Research (SPR) Program by the Tennessee Department of Transportation and the Federal Highway Administration under ***RES#:2019-18 Research Project Title: Evaluating Roadway Subsurface Drainage Practices.***

Technical Report Documentation Page

1. Report No. RES2019-18	2. Government Accession No.	3. Recipient's Catalog No.
4. Title and Subtitle *Evaluating Roadway Subsurface Drainage Practices*		5. Report Date Feb. 2022 6. Performing Organization Code
7. Author(s) Baoshan Huang, Qiang He, Christopher Wilson, Hang Lu, Pawel Polaczyk		8. Performing Organization Report No.
9. Performing Organization Name and Address University of Tennessee – Knoxville 851 Neyland Dr Knoxville, TN 37996		10. Work Unit No. (TRAIS) 11. Contract or Grant No. RES2019-18
12. Sponsoring Agency Name and Address Tennessee Department of Transportation 505 Deaderick Street, Suite 900 Nashville, TN 37243		13. Type of Report and Period Covered Final Report December 2018 – February 2022 14. Sponsoring Agency Code
15. Supplementary Notes Conducted in cooperation with the U.S. Department of Transportation, Federal Highway Administration.		

16. Abstract

Pavement drainage is a critical component in ensuring the good performance of the roadway. However, a lack of proper drainage design and inadequate materials frequently lead to insufficient pavement drainage ability. It is essential to establish reliable drainage design criteria for pavement structure and material choices. The objectives of this project were to identify critical areas in Tennessee that are prone to poor drainage, assess the performance of different drainage designs for critical areas, evaluate the performance of roadway designs, considering rainfall, penetration through pavement joints and cracks, and lateral seepage from ditches, and develop nomographs relating rainfall, hydropedological properties, time to drain, and pavement integrity. Based on the results, saturated hydraulic conductivity was quantified for the major soil types in Tennessee. The fair and poor pavement sections are mainly located in West Tennessee, with only a few weak spots in East Tennessee, corresponding to the distribution of soil with low hydraulic conductivity. Soil drainability significantly affects pavement performance, which can counteract the effect of precipitation and water table. Through a simple drainage calculator and a detailed simulation with ABAQUS, it was found that the permeabilities of the subgrade soil and aggregate base both affect roadway drainage, but in most cases, the subgrade soil has a much more significant influence on the drainage rates. Pavement dimensions such as base layer thickness, pavement width, and base slope affect pavement drainage ability. A nomograph was developed to check the compatibility of base and subgrade materials and pavement structural characteristics on ensuing pavement drainability. A flow chart was proposed for the implementation of the pavement drainage assessment.

17. Key Words Drainage; Pavement; Base; Subgrade; Hydraulic Conductivity; Precipitation	18. Distribution Statement No restriction. This document is available to the public from the sponsoring agency at the website https://www.tn.gov/.

19. Security Classif. (of this report) Unclassified	20. Security Classif. (of this page) Unclassified	21. No. of Pages 46	22. Price

Acknowledgments

This research was sponsored by the Tennessee Department of Transportation. The authors are indebted to Wesley Peck for serving as the Technical Advisor and providing productive input to improve this project. The authors would also like to thank Dr. Thanos Papanicolaou for his initial help with preparing this project and Dr. Wei Hu for his assistance with the falling head tests, as well as the following students and post-docs from the University of Tennessee: Dr. Hongren Gong, Miamiao Zhang, and Andrew Tsay.

Executive Summary

Poor subsurface drainability causes an accumulation of water within the aggregate base, reducing its strength. In many road sections, the aggregate material used for the base is obtained from local sources, while the in-situ soils are used for the subgrade. However, these in-situ soils and local materials are often insufficiently characterized in terms of drainability and may not satisfy the drainage needs at a site. This is particularly important in Tennessee, where the state has large land use, topography, and geology variability.

Due to the lack of guidelines that consider the effects of subgrade composition on the roadway drainage, this project conducted a comprehensive review of subgrade soils in Tennessee to identify areas exhibiting inefficient drainage, followed by an evaluation of the drainage for roadway designs in the state. Ultimately, nomographs were developed that relate different roadway design parameters, hydropedological properties, and pavement integrity.

Four different roadway surfaces, two types of aggregate bases, and three subgrade soils were selected with input from the Tennessee Department of Transportation (TDOT). For the aggregate bases, both limestone and chert were used. The three subgrade soils considered in this study consist of silt loam, silty clay loam, and loam soils. These three soil textures cover 89% of the state. To quantify saturated hydraulic conductivity, local soils were evaluated using standard methods. Then, the soil samples were compacted to a specified bulk density, 1.7 g/cm^3 for Loessal silts and 1.85 g/cm^3 for sandy silt clays. Falling head tests for the major soil types identified above were used to quantify saturated hydraulic conductivity, K_s, values determined using a pedotransfer function that considered texture, organic matter, and compaction-enhanced bulk densities. The silt loam soils had the lowest K_s (0.1986 ± 0.1387 µm/s) followed by silt clay loam (0.4139 ± 0.3727 µm/s) and loam (0.5405 ± 0.3962 µm/s) soils.

Additionally, the pavement roughness condition was correlated to different hydropedological properties. The pavement smoothness index (PSI) and international roughness index (IRI) for road segments in the four TDOT regions were used to categorize pavement roughness, while drainability, precipitation, and water table depth were correlated hydropedological parameters. The road segments classified as “Fair” or “Poor” are mainly located in West Tennessee, with only a few weak spots in East Tennessee, corresponding to the distribution of silt loam soils with low hydraulic conductivity. Soil drainability significantly affects pavement performance, which can counteract the effects of precipitation and water table.

Three sets of 72 simulations were conducted using a simple drainage calculator of two layers. The Time to Drain, T_d, was calculated as a function of the K_s of the aggregate and soil. The presence and condition of the edge drain proved to be an important characteristic controlling T_d. Without proper maintenance, the benefit of an edge drain is entirely negated. Grouping the data by subgrade soil type showed significant differences. Silt loam soils have the slowest saturated hydraulic conductivity of all soil types, and K_s is a sensitive term in the drainage calculator. The subgrade soil was the most influential factor that controlled the T_d values. The influence of the subgrade soil outweighed the influences of the edge drain condition, pavement surface type, and aggregate.

Detailed simulations with the Finite Element Method software, ABAQUS, were also performed to examine drainage of a whole pavement-aggregate-soil structure under a rainfall event. ABAQUS was also used to evaluate the influence of pavement width, base thickness, and base slope. The roadway's center section was the slowest drain during rainfall, while the shoulder was the fastest draining section. These locations were used as the critical locations to assess pavement drainability to see if the saturation level could drop from 100% to 50% in two hours. The relationship between saturation and permeability of base/soil was deduced from the results and the influence of pavement dimensions. Nomographs were drawn with these results, which benefit drainage design and assessment.

Laboratory experiments were conducted in a vertical column that included a surface pavement layer, an aggregate base, and a subgrade soil to verify the model results. The experiments simulated both the pavement shoulder and centerline. When the side drain worked well, the shoulder drained quickly to its residual saturation value in about an hour. The drainability of the soil below the shoulder influenced T_d by ~16%. However, the soil's influence at the centerline was minimal as the saturation level dropped to only 90% in the hour.

Based on the relationship between the base saturation and base/subgrade hydraulic conductivity, and the influence of pavement dimensions, a nomograph was developed to assess the compatibility of base and subgrade materials and pavement structural characteristics in ensuring the drainability of pavement. A flow chart for subsurface drainage assessment was drawn, incorporating the main findings of this project. The nomograph and the flow chart can be found in 4.6 and 4.7, respectively.

Key Findings

- Most of the pavement sections in Tennessee are in good condition, with a small portion in fair condition and some poor sections sporadically. The fair or poor sections are mainly located in West Tennessee, with only a few weak spots in East Tennessee.
- Subgrade soil is the most important characteristic influencing pavement drainability, which is supported by the following findings: a. Database analysis shows that soil drainability can be correlated with pavement condition. b. Database analysis shows soil drainability is more influential than high precipitation and shallow water tables. c. Simulation with a drainage calculator shows that the influence of the subgrade soil outweighed the influence of both the pavement surface and the aggregate type. d. Full-scale pavement drainage simulation gets the relationship of base saturation level and base/subgrade hydraulic conductivity, in which the subgrade parameter is much larger than the base parameter.
- Pavement drainability is influenced by the combination of base and subgrade material. Pavement dimensions, such as aggregate base thickness, pavement width, and base slope, also affect pavement drainability. The influence of these factors can be quantified and integrated into one equation. Surface hydraulic conductivity does not show a significant influence on pavement drainability.
- Based on the regressed equations concerning 2h drainage saturation, it is found that the TDOT base and subgrade materials can sometimes cause the drainability of pavement below the 2h-50% draining standard.

- The most vulnerable part of pavement during rainfall is the shoulder because the middle part of pavement is protected by surface structure. Rainfall entering through cracks or joints had limited effects on saturation levels. The saturation of pavement during rainfall is influenced by base/subgrade hydraulic conductivity but not significantly influenced by pavement dimension factors.
- Based on the regressed equation concerning saturation during heavy rainfall, it is found that TDOT base and subgrade materials rarely cause fully saturated pavements.

Key Recommendations

- If K_{soil} is too small (e.g., less than 0.00225 m/hr), chert is not recommended as the base material because of its low permeability.
- Aggregate base materials with a permeability large enough (e.g., larger than 44 m/hr) can be used with any subgrade soil type in Tennessee and still provide sufficient roadway drainage.
- It is recommended to check the compatibility of base and subgrade materials and pavement structural characteristics using the nomograph to ensure the drainability of pavement.
- For regions with greater precipitation and poor IRI history (especially for some areas of Region 4), the criteria for drainage assessment should be stricter.
- A comprehensive assessment should be done for any target pavement section, including quantitative assessment, qualitative assessment, and abnormity assessment.

Table of Contents

List of Tables

List of Figures

Chapter 1 Introduction

1.1 Problem statement

Pavement performance relates to porous media hydrology, as nearly 60% of premature pavement failures are triggered by inadequate drainage of the sublayers (Christopher and McGuffey, 1997). Poor subgrade soil drainage results in an accumulation of water within the aggregate base, reducing its strength. The prolonged presence of the water in the base also accelerates the deterioration of the above pavement through moisture warping (Wei et al., 2008), pothole formation (AASHTO, 2009), and reduction of the bearing capacity (Kuttah and Arvidsson, 2017).

An efficient drainage system is needed to avoid long periods of moisture retention, which lead to unsafe roads, high maintenance costs, and traffic delays (Schaefer et al., 2008). However, for convenience and to minimize costs of transporting graded aggregate from a quarry, the materials used for these lower layers are most often grabbed opportunistically from local sources. The local aggregate and in-situ soils used for the base and subgrade layers are often insufficiently characterized in terms of drainability and may not satisfy the drainage needs at a site. This is particularly important in Tennessee, where the state has an extensive land use, topography, and geology variability. A study comparing the spatial and temporal soil water extremes across Tennessee is essential for understanding the state's roadway drainage concerns.

Furthermore, expected increases in climate variability will result in higher rainfall throughout the state. Annual precipitation in West Tennessee is expected to increase by 11 mm under a moderate climate prediction scenario but may decrease by 18 mm under a more extreme climate scenario. In east Tennessee, annual precipitation is projected to increase by 47 mm under moderate and 24 mm under extreme climates. Seasonal changes are expected to be even higher (Wilson et al., 2022).

To work effectively, drainage systems must transport water from the point of infiltration to the drain outlet through aggregate, which has higher hydraulic conductivity than the subgrade soil. The drain and aggregate should be free of flow restrictions (Moulton, 1980). Due to the lack of guidelines regarding subgrade composition and its effects on roadway drainage in Tennessee, this project conducted the following tasks: identified areas exhibiting inefficient drainage through a comprehensive review of subgrade soils; evaluated roadway drainage design performance; and developed nomographs that relate different roadway design parameters, hydropedological properties, and pavement integrity. This project brings together geotechnical and hydraulic engineers, which is a rare composition and will contribute towards the sustainability of a "healthy" surface transportation system in Tennessee.

1.2 Objectives

This project addresses the following four objectives:

1) Identify critical areas in Tennessee that are prone to poor drainage.

2) Assess the performance of different drainage designs for critical areas in Tennessee with a drainage calculator.
3) Evaluate the performance of roadway designs, considering rainfall penetration through pavement joints and cracks, as well as lateral seepage from ditches.
4) Develop nomographs for roadway design considering rainfall, hydropedological properties, Time to Drain, and pavement integrity.

1.3 Report organization

The report is organized as follows: Chapter 2 introduces pavement drainage design practices, mechanisms of pavement hydrology, and the fundamental hydrology equations used in this project. Chapter 3 discusses the methodology used to address the objectives of this project, including experiments for measuring and verifying material (i.e., pavement; aggregate; soil) parameters, as well as two simulation methods. In Chapter 4, the results are presented for the pavement database analysis, experiments, and simulations. Furthermore, the design nomograph and accompanying recommendations are proposed. Chapter 5 concludes the study and offers suggestions for implementing the findings of this project.

Chapter 2 Literature Review

2.1 Pavement Drainage Design

The pavement structure for a roadway consists of a concrete or hot-mix asphalt surface, shoulder, aggregate base, subbase, and subgrade soil. To avoid failure, the pavement structure must quickly remove water through efficient drainage. Inefficient drainage stems from both poorly estimated geotechnical parameters and overlooked hydraulic parameters (NCHRP, 2001).

Drainage systems contain filter layers, trenches, ditches, and outlets (Figure 2-1). The drains are typically perforated pipes in the trenches, which are placed between the aggregate base and subgrade. Effective drainage systems can significantly extend pavement life when properly designed, constructed, and maintained. However, studies have shown that improperly designed, constructed, or maintained drainage systems could be worse than having no drain at all (Hassan and White, 1996; Christopher and McGuffey, 1997).

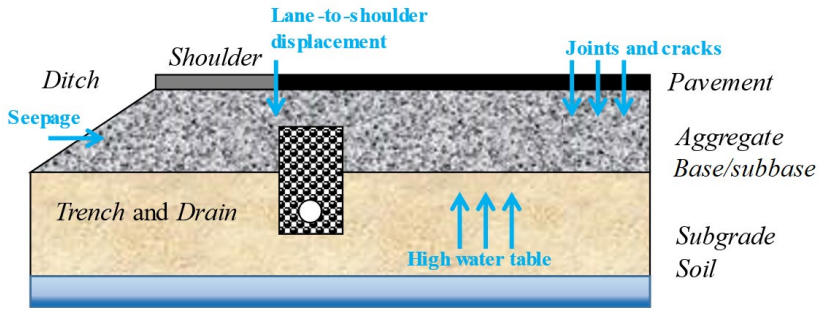

Figure 2-1. Schematic of pavement and drainage system components (not in scale). The arrows show the main flow pathways for water entering the pavement system.

Pavement drainage is usually designed based on key parameters, including the rate at which water enters the pavement, the hydraulic conductivity of the subbase material, and the ability of the drains to remove water (Huang, 2004).

The performance of the drainage system is evaluated using criteria like AASHTO's pavement drainage definitions (Table 2-1), although the performance may be influenced by additional factors other than drainage rate. This drainability rating ranges from "Excellent" to "Very Poor" and is correlated with the Time to Drain, T_d. According to AASHTO (1993), a drainage system is rated "Excellent" if the moisture, or saturation, level within the entire pavement system drops from 100% to 85% within 2 hours. However, previous studies have shown that current drainage systems do not always perform at such a high level of efficiency and, in some cases, have received a rating of "Very Poor" (Hossam et al., 1996; Daleiden, 1998).

Table 2-1. AASHTO definitions for pavement drainage.

Drainage Quality	Water Removal Time*
Excellent	2 hours
Good	1 day
Fair	1 week
Poor	1 month
Very Poor	Does Not Drain
* Based on time-to-drain; after Christopher et al. (2006)	

2.2 Pavement Hydrology

Water can enter the pavement sublayers through multiple mechanisms (Figure 2-1). Rain or snowmelt on the roadway surface can penetrate the pavement through joints and cracks or pass between the pavement and shoulder if lane-to-shoulder displacement has occurred (Christopher and McGuffey, 1997). This is usually the largest source of water to the roadway pavement system. Alternatively, high stormwater levels in adjacent drainage ditches can seep through the shoulder material following pressure gradients (i.e., lateral seepage). Groundwater can also enter via rising water tables (Huang, 2004).

While the water moves through the aggregate base, it can transport fine materials (e.g., sediment, road salt, and organic matter) to the drains. An excessive amount of fine material can clog the drains and prevent water flow (Figure 2-2). The high percentage of fine material in the drainage layer and other constituents is a common feature when the aggregate base layer is made from Recycled Portland Cement Concrete (White et al., 2008).

Figure 2-2. Example of a drain clogged with fine sediments from the drainage layer. From Bhattacharya et al., (2009).

Drainage through aggregate bases and subgrade soils can be characterized as saturated/ unsaturated flow through a porous medium. This process has been modeled using various methods, including algebraic relations, hydrologic budgets, and complex differential equations. The Richards equation provides a suitable framework to study the transient unsaturated flow through the different layers of granular materials in a gravel road (Mays, 2005).

The Richards equation is a modification of Darcy's Equation that assumes the hydraulic conductivity, *K*, is a function of the pressure head, *K(h)*:

$$q = -K(h)\,\nabla H \tag{2-1}$$

where *q* is the groundwater flux; and *H* is the total head change.

If the Richards equation is applied to a domain that contains both areas of saturated and unsaturated flow (i.e., a draining pavement-aggregate-soil structure), the following equation is used to conduct a volume balance of the flow:

$$\int_A^0 K(h)\ \times n\ dA = \frac{d}{dt}\ \int_V^0 \theta(h) dV \tag{2-2}$$

where *A* is the area; *V* is the volume; and *t* is time. In the saturated region of the domain, *h* is greater than 0, and the saturated hydraulic conductivity values and moisture content are used. In the unsaturated portion, *h* is less than 0, and the following mixed form of the Richards equation is derived from Equation 2-2 to account for the transition from unsaturated to saturated flow.

$$\frac{\delta\theta}{\delta t}\ =\ \nabla\ \cdot (K(h)\nabla h) + \frac{\delta K}{\delta z} \tag{2-3}$$

where θ is the water content; *K* is the hydraulic conductivity; *h* is the pressure head; and *t* and *z* are the time and vertical coordinates, respectively. In the context of subsurface drainage, the changing water content concerning time is the rate at which water leaves the aggregate base and subgrade soil.

Thus, the hydraulic conductivity and the pressure head are the key parameters for determining the temporal evolution of water content in porous media. However, Equation 2-3 must be coupled with auxiliary relationships (e.g., Brooks and Corey, 1964) to express the dependency of *K* and *h* on θ. The Brooks-Corey relations follow as:

$$\begin{cases} K(\theta) = K_s \left(\frac{\theta-\theta_{res}}{\theta_{sat}-\theta_{res}}\right)^{\lambda_2} \\ h(\theta) = h_d \left(\frac{\theta-\theta_{res}}{\theta_{sat}-\theta_{res}}\right)^{-\frac{1}{\lambda_1}} \end{cases} \tag{2-4}$$

where K_s is the saturated hydraulic conductivity; θ_{res} is the residual water content; θ_{sat} is the saturated water content; h_d is the bubbling pressure (which is the minimum capillary pressure in the porous medium); λ_1 is the pore-size index; and λ_2 is a fitting parameter. In total, the two parts of Equation 2-4 provide 6 parameters (namely, K_s, θ_{res}, θ_{sat}, h_d, λ_1, λ_2) that can describe the physical properties of the granular materials affecting the movement of water through a porous medium under unsaturated conditions.

Hydrologic parameters, including those in Equation 2-4, have been linked to several pedologic properties, such as soil texture and bulk density, through empirical relationships or pedotransfer functions (Pachepsky et al., 2006). Relationships, like the following, have been developed for determining K_s using different combinations of soil properties (e.g., Wosten et al., 1999; Maidment, 1993; Papanicolaou et al., 2015b; Elhakeem et al., 2018):

$$K_s = 0.7919 + (0.001691 \times C) - (0.29619 \times BD) - (0.000001491 \times S^2) + (0.0000821 \times OM^2) + (0.02427 \times C^{-1}) + (0.01113 \times S^{-1}) + (0.01472 \times \ln S) - (0.0000733 \times OM \times C) - (0.000619 \times BD \times C) - (0.001183 \times BD \times OM) - (0.0001664 \times S) \quad (2\text{-}5)$$

where *C* is the clay content; *BD* is the bulk density; *S* is the silt content; and *OM* is the organic matter content.

The saturated water content coincides with the porosity, *φ*, of the material. The porosity can be estimated with the bulk density and the particle density, *PD*, using the following formula:

$$\phi = 1 - \frac{BD}{PD} \quad (2\text{-}6)$$

The residual water content, bubbling pressure, and pore-size index can be estimated using the porosity as well as the silt and clay contents with the following formulae (Maidment, 1993):

$$\theta_{res} = -0.0182482 + (0.00087269 \times \mathrm{S}) + (0.00513488 \times \mathrm{C}) + (0.02939286 \times \phi) - (0.00015395 \times \mathrm{C}^2) - (0.0010827 \times \mathrm{S} \times \phi) - (0.00018233 \times \mathrm{C}^2 \times \phi^2) + (0.00030703 \times \mathrm{C}^2 \times \phi) - (0.0023584 \times \phi^2 \times \mathrm{C}) \quad (2\text{-}7)$$

$$h_d = -\exp(5.3396738 + (0.1845038 \times \mathrm{C}) - (2.48394546 \times \phi) - (0.00213853 \times \mathrm{C}^2) - (0.04356349 \times \mathrm{S} \times \phi) - (0.61745089 \times \mathrm{C} \times \phi) + (0.00143598 \times \mathrm{S}^2 \times \phi^2) - (0.00855375 \times \mathrm{C}^2 \times \phi^2) - (0.00001282 \times \mathrm{S}^2 \times \mathrm{C}) + (0.00895359 \times \mathrm{C}^2 \times \phi) - (0.00072472 \times \mathrm{S}^2 \times \phi) + (0.0000054 \times \mathrm{C}^2 \times \mathrm{S}) + (0.5002806 \times \phi^2 \times \mathrm{C})) \quad (2\text{-}8)$$

$$\lambda_1 = \exp(-0.7842831 + (0.0177544 \times \mathrm{S}) - (1.062498 \times \phi) - (0.00005304 \times \mathrm{S}^2) - (0.00273493 \times \mathrm{C}^2) + (1.11134946 \times \phi^2) - (0.03088295 \times \mathrm{S} \times \phi) + (0.00026587 \times \mathrm{S}^2 \times \phi^2) - (0.00610522 \times \mathrm{C}^2 \times \phi^2) - (0.00000235 \times \mathrm{S}^2 \times \mathrm{C}) + (0.00798746 \times \mathrm{C}^2 \times \phi) - (0.00674491 \times \phi^2 \times \mathrm{C})) \quad (2\text{-}9)$$

The fitting parameter, λ_2, is related to the pore-size index through the formula:

$$\lambda_2 = \frac{2+3\lambda_1}{\lambda_1} \quad (2\text{-}10)$$

Once the above parameters have been provided, Equation 2-4 can be solved numerically to quantify the changing water content in the subbase and subgrade.

The Time to Drain, T_d, for a particular soil is related to its saturated hydraulic conductivity, which can provide a basis for developing a nomograph-based assessment of roadway drainage. A lower K_s value signifies the slower water movement through soil and a longer T_d. K_s is a hydropedological property that is a function of soil texture and bulk density, as well as land use and weather shifts. Thus, the drainability of a subgrade varies spatially based on soil type, and it will change as the soil becomes compacted during roadway construction. Drainability will also vary temporally by season. K_s can therefore reflect a range of changes in T_d under different conditions.

Chapter 3 Methodology

3.1 Geotechnical Examinations

Standard methods of ASTM International and other geotechnical methods were used to evaluate the characteristics of representative soils from the state. The soil samples were air-dried at room temperature under low humidity for one week and weighed. The bulk density was determined by dividing the dry weight by the sample volume (125 cm^3).

For texture, the soil was lightly crushed and passed through a nest of pre-weighed sieves (i.e., No. 10, 20, 40, 60, 100, 140, 200) to determine the sand content (ASTM D422). The silt-clay particle size distribution was determined using a standard hydrometer test (ASTM D422-63). Approximately 50 g of the soil, less than 0.074 mm, was dispersed in 125 mL of a 35.7 g/L mixture of sodium hexametaphosphate $(NaPO_3)_6$ for 12 hours. Hydrometer measurements were recorded at intervals over two days to determine fine soil particles' gradation.

The textures of the soils were confirmed using a split of 5 g and a Coulter Particle Size Counter (ASTM D422-63). The split was prepared with additions of deionized water, hydrogen peroxide, acetic acid, and sodium hexametaphosphate. A serial dilution of up to 105 mL was conducted to detect particles ranging from 0.020 – 0.074 mm.

The Liquid Limit (LL) and Plastic Limit (PL) were estimated using the Casagrande Cup method and the standard plastic limit test (ASTM D4318). The Plasticity Index, PI, was estimated as the difference between the LL and the PL, or PI = LL – PL. The organic carbon was measured using a visible near-infrared spectrometer following the NRCS Rapid Carbon Assessment protocol. The pH of each sample was measured in a 1:2 mixture with distilled water.

3.2 Falling-Head Tests

For the Falling Head Test, the sample was compacted to a bulk density of 1.7 g/cm^3 for loessal silt loams and 1.85 g/cm^3 for the silty clay loams and loams by mixing about 3 kg of the soil and 460 g of water. The soil was molded into a cylinder with a radius of 3.5 cm using a compactor, and the samples' heights ranged from 9 – 11 cm.

After compaction, the soils were placed in a permeameter. The permeameter had four main components: an air valve, loading platform, nozzle, and graduated cylinder. The sample was placed on the loading platform and saturated with water. The graduated cylinder was attached overtop. Two rods were fastened to the sides to keep the lid in place. The air valve was pumped to create pressure within the sample chamber.

Water was poured into the graduated cylinder, and the height was recorded as the initial value. The nozzle was opened, and as the water level in the graduated cylinder dropped, its level and the current time were recorded to calculate the hydraulic conductivity.

3.3 Correlation between Soil Drainability and Pavement Condition

The Tennessee Department of Transportation maintains a Pavement Management System database, which holds health metrics for the interstates, state highways, and county roads in

the state. The International Roughness Index (IRI) and the Pavement Smoothness Index (PSI) were used to evaluate pavement conditions in response to the roadway drainage.

The IRI is a commonly used road roughness index determined from a 2-dimensional road profile showing elevation as it varies with longitudinal distance. The U.S. Federal Highway Administration (FHWA) considers roadways with IRI values less than 1.50 m/km in "good" condition. Roadways with IRI values ranging from 1.51 to 2.68 m/km are considered "fair" and should be monitored regularly for further deterioration. Those roads with values greater than 2.68 m/km are considered "poor," making them a high priority for rehabilitation.

The PSI measures the roughness of the road as the deviation of a pavement surface from an actual planar surface while examining the longitudinal profile, transverse profile, and cross slope. The metric uses a scale ranging from 0 to 5, and Table 3-1 illustrates the limits of PSI. The PSI is related to the IRI (Long, 2017) in the following:

$$PSI = 5 \times e^{(-0.0055 \times IRI)} \tag{3-1}$$

Table 3-1. PSI evaluation levels.

Levels	Interstates	State Routes
Good	PSI $\geq$ 3	PSI $\geq$ 2.6
Fair	2.6 $\leq$ PSI < 3	2.2 $\leq$ PSI < 2.6
Poor	PSI < 2.6	PSI <2.2

3.4 Drainage Calculator

For the drainage calculator, a two-dimensional domain of a roadway was covered by a mesh of triangular elements with node points at the vertices (Figure 3-1). The domain dimensions were entered via excel, and the elements were positioned, so the interfaces between the two layers were along their edges.

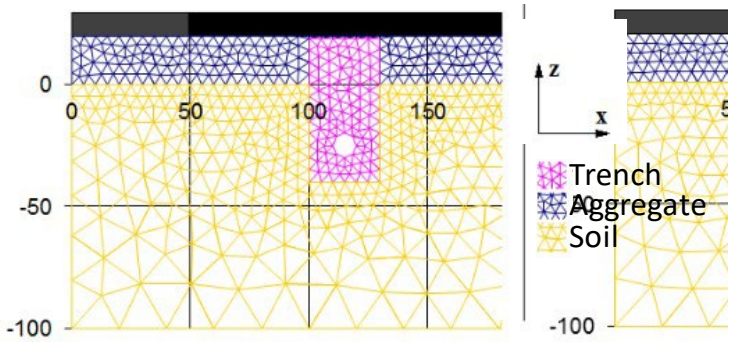

Figure 3-1. Example of the mesh generated with the drainage calculator. The domain contains the aggregate base, subgrade soil, and trench with the edge drain.

Four different roadway surfaces, two types of aggregate bases, and three subgrade soils were selected with input from TDOT (Table 3-2). The four roadway surfaces are comprised of asphalt layers (with and without an A-S drainage layer) and concrete (with and without an A-S drainage layer). For the aggregate bases, both limestone and chert were used. The limestone layer is more prevalent in the western part of Tennessee, while the chert layer is found in the eastern

part. The three subgrades used in this study consist of silt loam, silty clay loam, and loam soils. These three soil textures cover 89% of the soil in the state. Because the drainage calculator has a two-layer domain, the pavement surfaces and aggregate bases were grouped as the upper layer. At the same time, the subgrade soils were considered the lower layer. Depth-weighted averages based on different surface-aggregate hydraulic and geotechnical properties were used to define the upper layer.

Table 3-2. Roadway Surfaces, Aggregate Bases, and Soil Subgrades.

Roadway Surfaces	
1	Asphalt: D layer (3.18 cm); BM2 layer (5.08 cm); A layer (15.2 cm)
2	Asphalt: D layer (3.18 cm); BM2 layer (5.08 cm); A layer (7.62 cm); A-S layer (7.62 cm)
3	Portland Cement Concrete: PCC (25.4 cm)
4	Portland Cement Concrete: PCC (25.4 cm); A-S (15.2 cm)
Aggregate	
1	Chert (25.4 cm)
2	Limestone (25.4 cm)
Soil	
1	Silt Loam
2	Silty Clay Loam
3	Loam
Edge drain	
1	No edge drain
2	Edge drain
3	Fouled edge drain

Three sets of 72 simulations were conducted using the drainage calculator. Each pavement-aggregate-soil combination was simulated for three different drainage cases. In the first case, no edge drain was present in the modeling domain, while an edge drain was present in the second and third cases. The second case used a clean edge drain, and the third case used an edge drain filled with fine particles. All combinations of 4 surfaces, 2 aggregates, 3 soils, and 3 drain cases multiply to a total of 72 simulation models.

For solving the Richards equation (Equations 2-3 and 2-4), the three sets of 72 simulations used input parameters (Table 3-3) that cover the range of saturated hydraulic conductivity values for each layer (e.g., upper quartile, median, lower quartile). To identify the physical ranges of saturated hydraulic conductivity and the other parameters in the Richards equation, SSURGO data for the inherent properties of the soils in the state (i.e., texture, organic matter content; bulk density) were utilized. In addition, pavement, transportation, and hydropedological literature sources were examined (Rawls, 1992; Meyer et al., 1997; Schaap et al., 2003; Voller, 2003; Gupta et al., 2004; White et al., 2009; Pease, 2010; Norambuena-Conteras et al., 2013; Wang et al., 2013; Nokkaew, 2014; Aboufoul and Garcia, 2017; Ellithy, 2017) for the needed input parameters used in Equation 2-5 – Equation 2-10.

Table 3-3. Input Parameters for Drainage Calculator.

Parameter	λ_1	θ_{sat}	θ_{res}	h_d (cm)	K_s (cm/s)	λ_2
PCC max	1.296	0.297	0.030	-5.327	2.31E+00	1.967
PCC mean	1.173	0.241	0.030	-5.617	1.11E+00	2.631
PCC min	0.583	0.152	0.030	-5.845	4.00E-02	7.285
D max	0.173	0.180	0.010	-4.820	8.50E-05	15.352
D mean	0.100	0.167	0.010	-4.963	5.20E-06	19.015
D min	0.052	0.156	0.010	-5.141	1.90E-07	23.354
BM2 max	0.182	0.205	0.010	-4.820	1.10E-04	15.014
BM2 mean	0.122	0.167	0.010	-4.972	1.40E-05	17.717
BM2 min	0.084	0.156	0.010	-5.491	2.20E-06	20.143
A max	0.531	0.374	0.010	-5.541	2.50E-02	7.901
A mean	0.357	0.247	0.010	-5.667	3.30E-03	10.555
A min	0.186	0.212	0.010	-6.121	1.20E-04	14.900
A/S max	0.908	0.521	0.010	-5.960	3.80E-01	4.333
A/S mean	0.551	0.329	0.010	-6.073	3.00E-02	7.662
A/S min	0.340	0.361	0.010	-6.646	2.60E-03	10.868
Chert max	0.753	0.320	0.010	-4.800	9.77E-01	5.790
Chert mean	0.654	0.250	0.010	-5.196	3.23E-01	6.299
Chert min	0.533	0.174	0.010	-5.770	6.47E-02	7.117
Limestone max	0.819	0.371	0.010	-4.563	1.90E+00	5.505
Limestone mean	0.698	0.280	0.010	-5.012	5.40E-01	6.057
Limestone min	0.501	0.156	0.010	-5.942	4.00E-02	7.382
Silt Loam max	0.139	0.582	0.015	-32.22	2.98E-05	17.06
Silt Loam mean	0.123	0.485	0.055	-35.19	1.89E-05	18.12
Silt Loam min	0.113	0.420	0.100	-37.37	1.36E-05	18.90
Silty Clay Loam max	0.176	0.524	0.060	-26.31	7.39E-05	14.95
Silty Clay Loam mean	0.154	0.477	0.095	-29.60	4.46E-05	16.13
Silty Clay Loam min	0.139	0.418	0.116	-32.10	3.04E-05	17.02
Loam max	0.180	0.551	0.027	-25.72	8.09E-05	14.74
Loam mean	0.169	0.451	0.080	-27.33	6.32E-05	15.32
Loam min	0.161	0.375	0.107	-28.46	5.32E-05	15.72

To solve Equation 2-4, the six hydraulic parameters (K_s, θ_{res}, θ_{sat}, h_d, λ_1, λ_2) were supplied for the two layers. The hydraulic conductivities and pressure heads were then used by the drainage calculator to solve the mixed form of the Richards equation (Eq. 2-3) using a control volume finite element method (Voller, 2003; Papanicolaou et al., 2015b). Starting from a completely saturated system, the change in water content is solved with respect to the conductivity as a function of the total head.

3.5 Full-Scale Pavement Drainage Simulation

For further understanding of moisture movement in the pavement system, ABAQUS simulations were performed. ABAQUS can solve most geotechnical engineering problems, including consolidation, seepage, and failure/ post-failure analysis. Compared to the drainage calculator, ABAQUS can investigate the influence of rainfall and the presence of cracks. The pavement structure in ABAQUS was created using real dimensions of the Tennessee pavement structure (Figure 3-2). The material and thickness characteristics of each layer are in Tables 3-2 and 3-3.

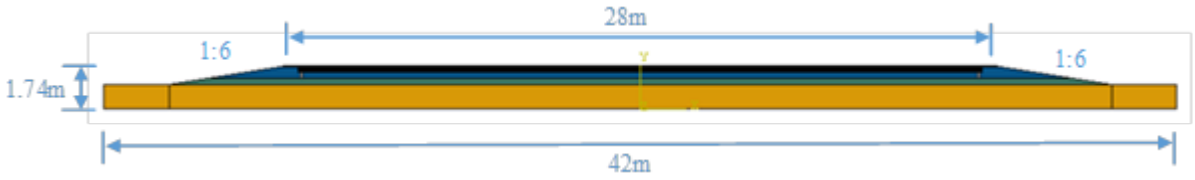

Figure 3-1. The pavement domain for the ABAQUS simulations.

The whole pavement structure was initially set at full saturation and was allowed to drain for 24 hours, which was presumed to be a stable saturation level. Rainfall was applied for the next 72 hours, following the pattern in Figure 3-3. For 24 hours, it gradually increased to a peak (50mm/h). Then it maintained the peak for the next 24 hours and gradually decreased for the final 24 hours. For asphalt pavement, a crack was set at the centerline with a width of 10 mm, and rain falls through the crack and directly on the base aggregate, as shown in Figure 3-4.

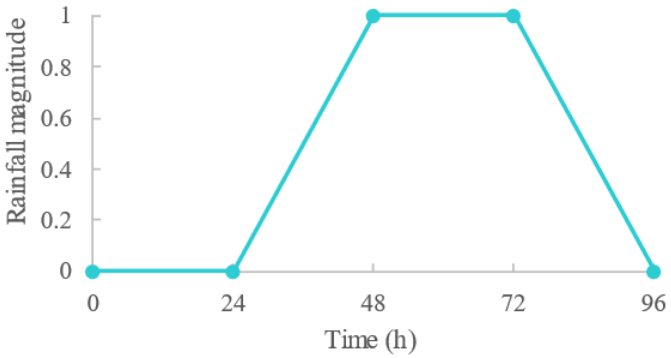

Figure 3-2. Simulated rainfall pattern for the ABAQUS simulations.

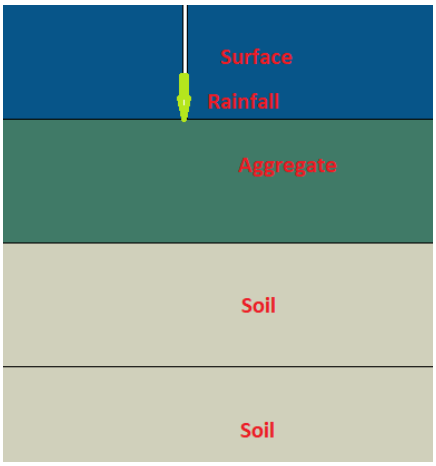

Figure 3-3. Location of the crack in the pavement structure.

3.6 Laboratory Experiment of Pavement Drainage Simulation

Laboratory experiments to verify the results of the ABAQUS simulations were performed in a PVC column with a 6-inch diameter allowing for the use of the soil molded with the pavement compactor (Figure 3-5 and Figure 3-6). Pavement layers were placed in the column, including the surface layers, aggregate base, and subgrade soil. The compacted soil was put into the pipe with aggregate loaded directly from the top and taped with iron bars to compact it. A surface asphalt mixture was pre-molded and placed in three layers overtop the aggregate. Full saturation was established as the initial state by closing all the drainage outlets as the water was poured into the column. The pavement structure was considered fully saturated when the water started to accumulate on the surface and no longer infiltrated. The drainage outlets were opened, and the water content in the aggregate and soil layers was measured every 10 minutes for 2 hours using moisture sensors (i.e., water content reflectometers).

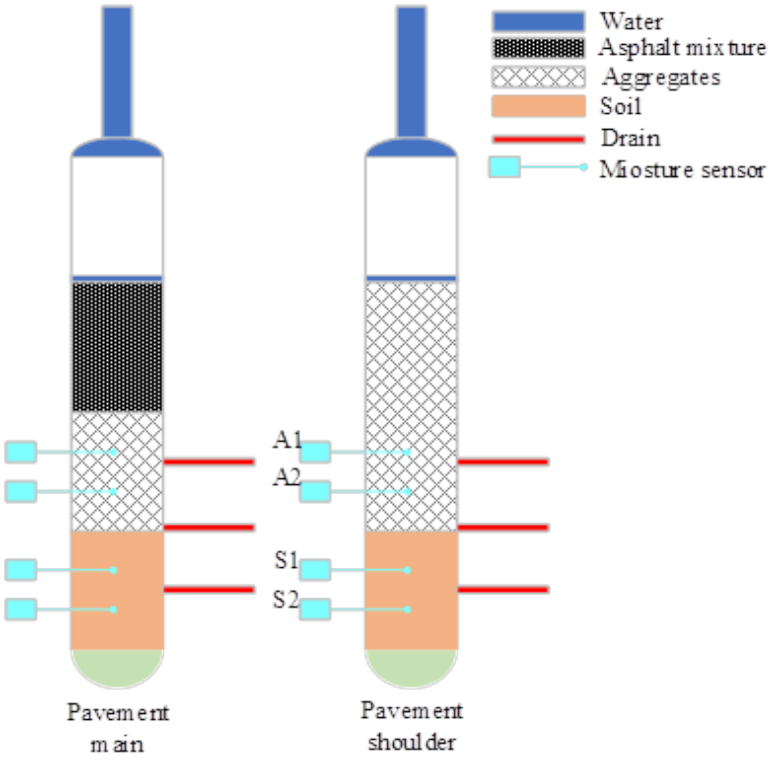

Figure 3-4. Schematic of the experimental set-up.

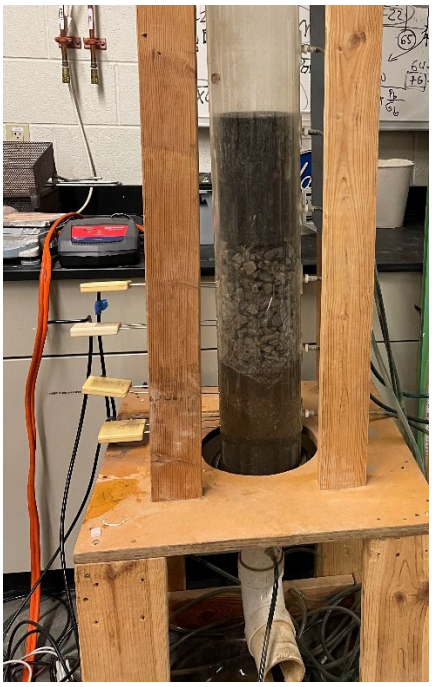

Figure 3-5. Real image of the experimental drainage column.

Chapter 4 Results and Discussion

4.1 Soils in Tennessee

County-level data from the Soil Survey Geographic Database (SSURGO) by the Natural Resources Conservation Service were mined for the properties of the soils in the state (i.e., texture, organic matter content; bulk density). The goal was to identify the soil types most likely to experience poor drainage by quantifying infiltration and saturated hydraulic conductivity using pedotransfer functions, like Equation 2-5.

Equation 2-5 was selected as it has proven to be robust in past studies using loess-derived soils (Wosten et al., 1999; Papanicolaou et al., 2015a; 2015b; Elhakeem et al., 2018; Wilson, 2021). More importantly, Equation 2-5 considers the effects of bulk density on saturated hydraulic conductivity, texture, and organic matter. Since this study dealt with compacted subgrade soils, including bulk density seemed mandatory.

There are seven major soil types in the state, namely silt loam (64%), loam (16%), silty clay loam (9%), sandy loam (8%), clay loam (1%), silty clay (1%), and clay (1%). The soil types with the highest capacity to store water (Figure 4-1) include silt loam, silty clay loam, and loam, which are most abundant in Tennessee. "Available water" is the difference between field capacity and permanent wilting point. It reflects how much water the soil can hold. "Field capacity" is the maximum amount of water that soil can hold against gravity, and "permanent wilting point" is the moisture content at which it can no longer sustain plants. The ability to store water reflects drainability (i.e., Time to Drain, T_d; saturated hydraulic conductivity, K_s). Typically, soils with the highest water holding capacities (e.g., silt loam) have the lowest K_s (Rawls, 1992; Pachepsky et al., 2006). These soils are most likely to drain poorly, resulting in poor pavement conditions.

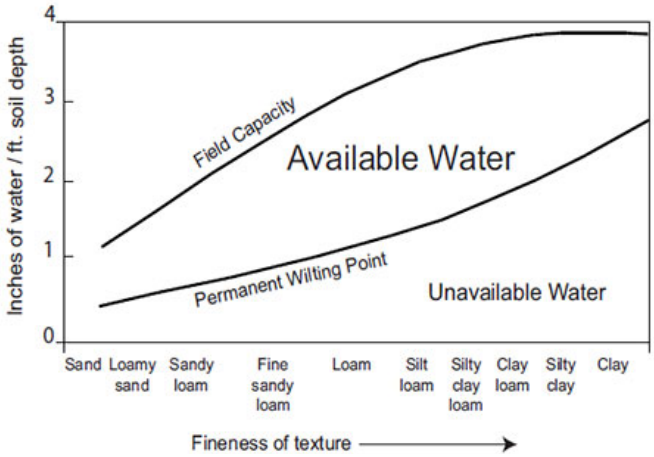

Figure 4-1. Relationship between texture and available water. From Ohio Agronomy Guide, 14th ed. Bulletin.

For all soil pedons in the state, the saturated hydraulic conductivities were determined based on the textural data from SSURGO and the proctor density values (Wagner et al., 1994; Nhantumbo and Cambule, 2006). Table 4-1 shows the harmonic mean values and standard deviations of the K_s values per soil texture. The harmonic mean is more applicable for log-normally distributed rate values, like K_s (e.g., Papanicolaou et al., 2015b; Elhakeem et al., 2018).

For the soils in Tennessee, those with a silt loam texture tended to have the slowest K_s values. Moreover, the silty clay loam and loam soils also had some of the slowest average K_s values. As these three soil textures are overwhelmingly abundant in Tennessee (covering 89% of the state), many of the state's soils are likely to be poorly drained.

Table 4-1. Saturated hydraulic conductivity values per soil type.

Texture	Harmonic Mean ± Standard Deviation (µm/s)
Silt loam	0.1986 ± 0.1387
Silt	0.2130 ± 0.0399
Silty clay loam	0.4139 ± 0.3727
Loam	0.5405 ± 0.3962
Silty clay	0.6096 ± 0.5476
Clay	0.6442 ± 0.6467
Clay loam	1.029 ± 0.6074
Sandy clay loam	1.077 ± 0.5601
Sandy loam	1.342 ± 1.394
Sandy clay	2.210 ± 1.479
Loamy fine sand	2.311 ± 3.678
Sand	6.792 ± 11.26

Figure 4-2 shows a map of K_s values for the state of Tennessee, which were determined using Equation 2-5. The regions colored in light or dark orange with the lowest K_s values were typically silt loam soils. The orange areas increased, moving from the state's center to the west. This included the large swath of loess-derived, silty soils in west Tennessee. It will be shown later that this area will also have the highest percentage of roadways classified as "Poor" due to moisture-induced roughness problems.

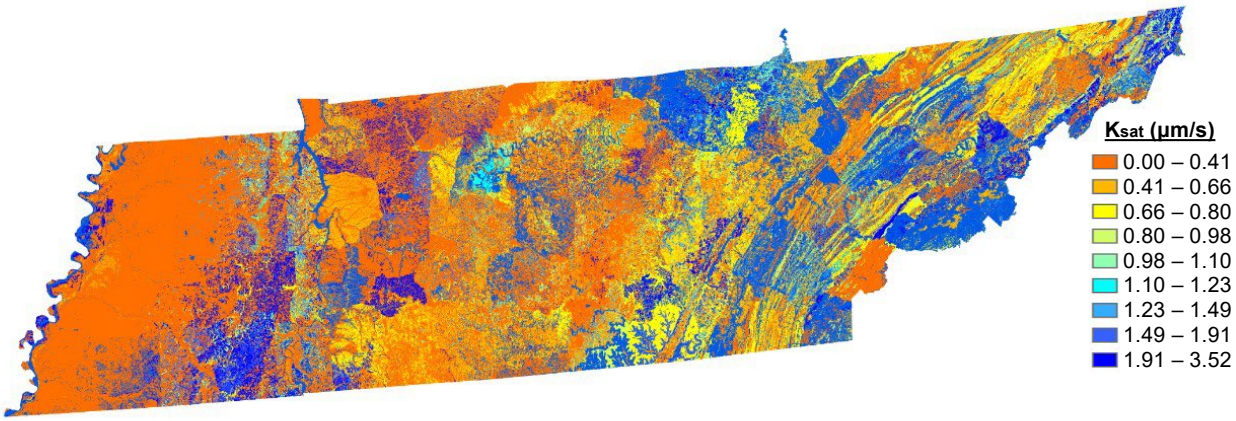

Figure 4-2. Map of the saturated hydraulic conductivity values throughout Tennessee.

Soil samples from the east (i.e., Knoxville) and west (i.e., Memphis) Tennessee, were characterized for their bulk properties of texture, bulk density, organic matter content, and Atterberg Limits. The texture results suggested that there were 3 silt loam samples, 3 silty clay

loam samples, and 3 loam samples. The Atterberg limit tests suggested that the silt loam samples had a liquid limit of 32% and a plasticity index of 8%. The silty clay loam samples had a liquid limit of 37% and a plasticity index of 17%. The loam soils had a liquid limit of 42% and a plasticity index of 20%. Proctor density tests showed the maximum density of the silt loams was 1.7 g/cm$^{\wedge 3}$, with a moisture content of 15%. The maximum density of the sandier soils (i.e., silty clay loams and loams) was 1.85 g/cm$^{\wedge 3}$ with 17% moisture content.

Falling head tests for the soil samples were used to measure saturated hydraulic conductivity and verify the values determined with Equation 2-5. For the silt loam soils, the average K_s was 3.07 X 10$^{\wedge -2}$ ± 2.05 X 10$^{\wedge -2}$ µm/s. For the silt clay loam soils, K_s averaged 1.08 X 10$^{\wedge -2}$ ± 6.03 X 10$^{\wedge -2}$ µm/s. For the loam soils, K_s was 4.08 X 10$^{\wedge -1}$ ± 3.21 X 10$^{\wedge -8}$ µm/s.

4.2 Correlation between Soil Drainability and Pavement Condition

Pavement condition data from the TDOT Pavement Management System and soil drainability were compared to identify if a correlation existed between them. Figure 4-3 shows the relationship between soil drainage properties and PSI. The pavement sections in "Good" condition had the highest median soil drainability, while the pavements in "Poor" condition had the lowest median soil drainage drainability. Thus, higher soil drainability generally translated to better pavement performance; however, there was substantial overlap in soil drainability across different pavement conditions, which yielded no significant relationship between soil drainability and PSI. Pavement performance is a complex phenomenon that is influenced by many factors, not just the soil drainability, such as pavement age, base material differences, etc. A lack of database of other factors makes comprehensive analysis considering all factors impossible. However, as the amount of data is great enough, the mean values from the big data analysis can still show preliminary facts.

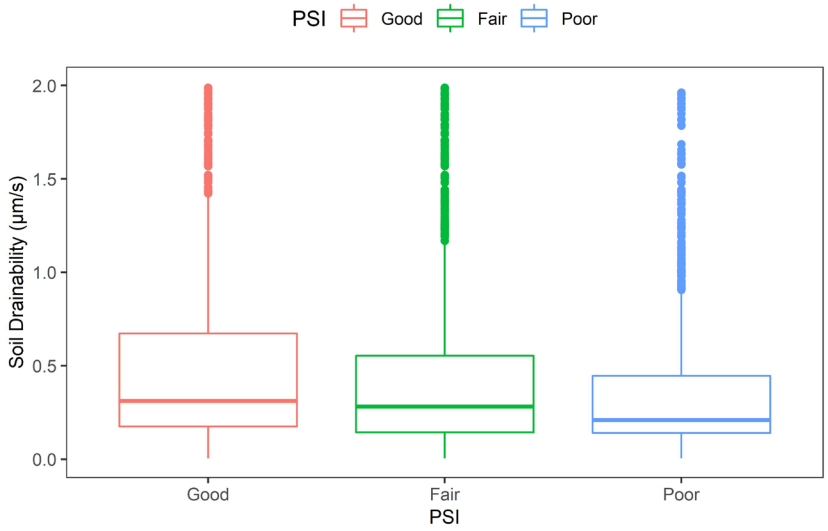

Figure 4-3. Relationship between soil drainability and PSI.

Most pavement sections in Tennessee are in "Good" condition (Figure 4-4). Most "Fair" and "Poor" pavement sections are in west Tennessee.

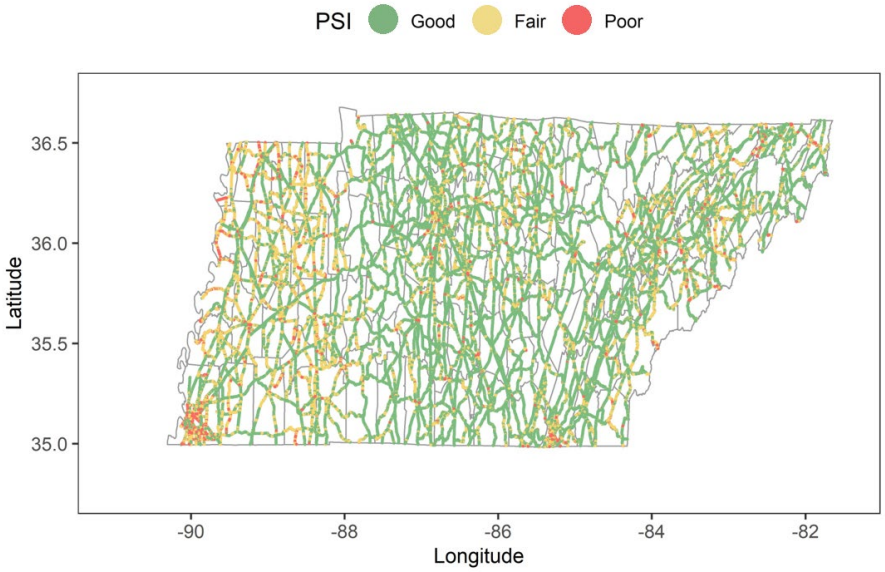

Figure 4-4. PSI map in Tennessee.

The relationship between roadway surface condition and drainability is more evident in Figure 4-5. Colored lines are 0.1-mile road segments with International Roughness Index (IRI) values corresponding to the "Poor" classification. These segments appear most abundantly in areas of the state with silt loam soils and low K_s values (i.e., areas of light grey).

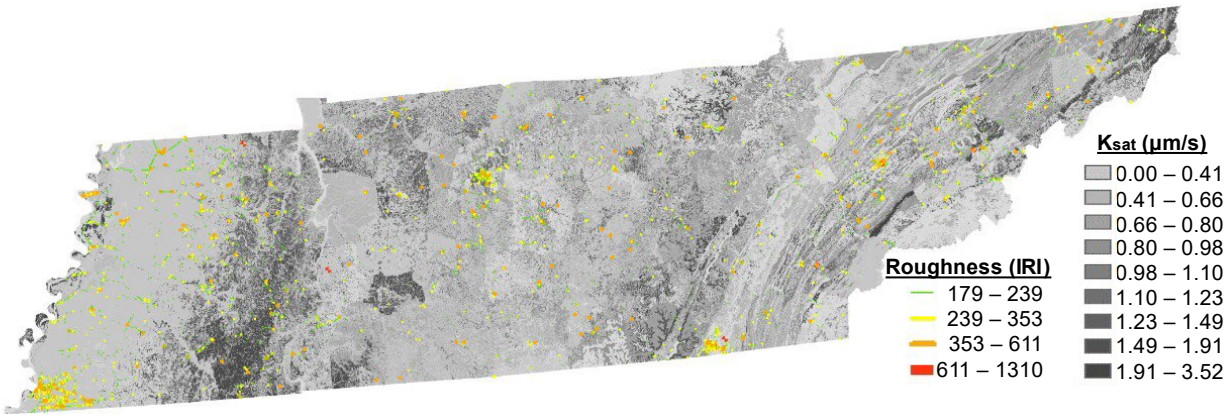

Figure 4-5. Map of IRI and K_s.

Given the apparent geographic differences in pavement conditions, the four TDOT regions were explored more closely regarding soil drainability, precipitation, water table depth, and IRI (Figure 4-6). Soil drainability decreases from east to west or from Region 1 to Region 4. The precipitation amounts in Regions 2 and 4 are generally more significant than in Regions 1 and 3, while the water table depths in Regions 2 and 4 are generally shallower than in Regions 1 and 3. Thus, it could be deduced that the pavement performance in Regions 2 and 4 would be worse, having higher IRI. Region 4 has the highest median IRI, but the median IRI in Region 2 is lower than in Region 4. Examining the soil drainability shows that the soils in Region 2 are more well-drained than those in Region 4, which have the lowest drainability values. Precipitation and soil drainability influence pavement performance, but soil drainability has a higher impact.

High precipitation and poor drainability are associated with higher levels of pavement distress (Region 4), but high precipitation and good drainability yield lower levels of distress (Region 2).

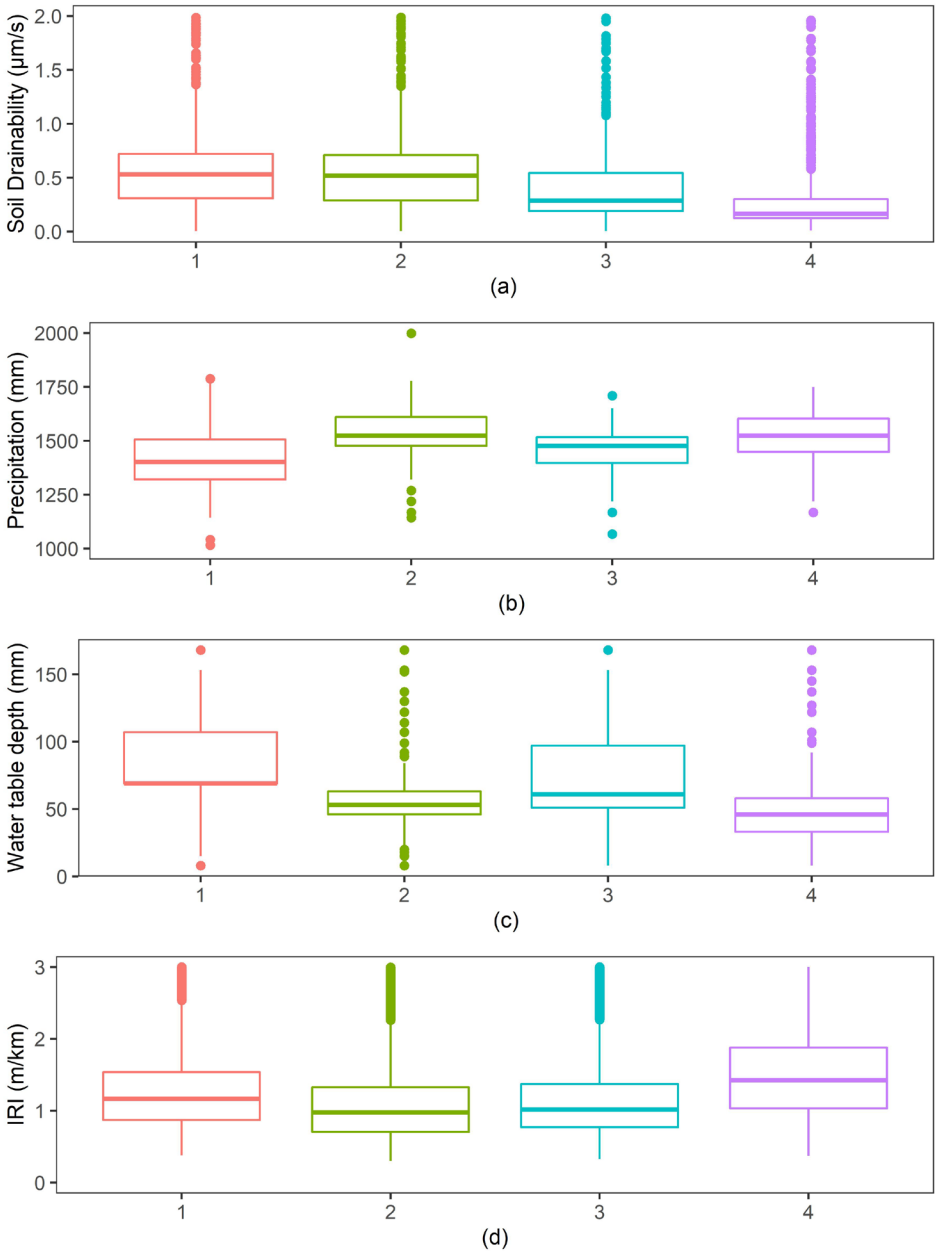

Figure 4-6. Comprehensive comparison between TDOT regions.

4.3 Assessment of Drainage Design with Drainage Calculator

4.3.1 Drainage calculation results and discussion

To assess roadway drainage performance, it is important to understand the change in water content over time ($\delta\theta / \delta t$) for the whole pavement-aggregate-soil system. The Richards equation, which combines Darcy's law with the conservation of mass, provides a suitable

framework to quantify transient unsaturated flow through the granular layers of the aggregate and subgrade soil (Mays, 2005).

The drainage calculator used a control volume finite element solution of the Richards equation to quantify the simultaneous change in water content over time for a two-layer domain (Voller, 2003; Papanicolaou et al., 2015b). The $\delta\theta / \delta t$ was used to determine the Degree of Saturation, S_w, and Time to Drain, T_d, of the upper layer (i.e., combined pavement-aggregate layer), which is dictated by the drainability of the lower layer (i.e., subgrade soil).

The presence and condition of the edge drain proved to be critical factors for determining T_d. The simulations that considered the presence of a clean edge drain were the only cases in which S_w of the upper layer reached their residual moisture levels (i.e., <5%) within 96 hours (Figure 4-7). The T_d values ranged between 37 and 67 hours.

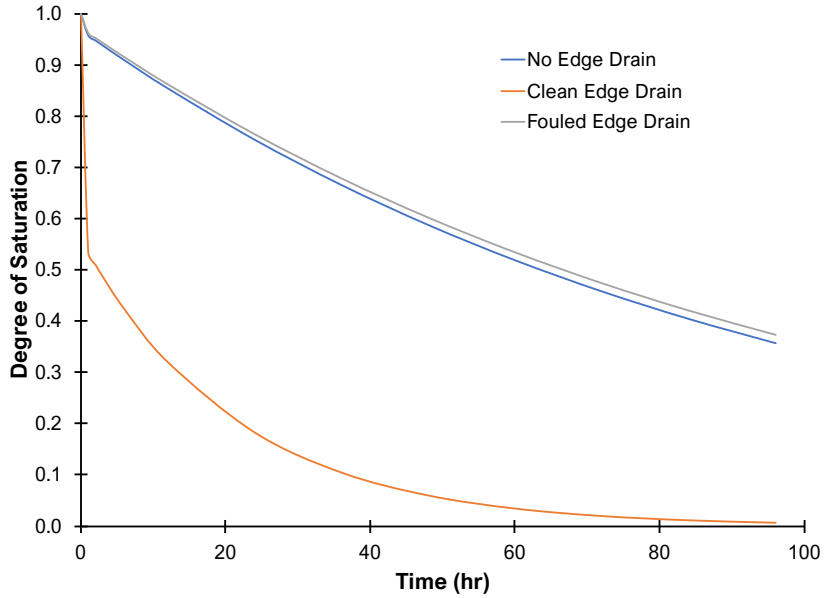

Figure 4-7. Change in the degree of saturation over a 96-hour simulation for three different drainage conditions.

Those simulations with no edge drain had an average S_w of 24% ± 15% at the end of the 96-hour simulation. The runs using a fouled edge drain had an average final S_w of 27% ± 15%. There was no significant difference between these two sets of simulations (T-test; p = 0.54), highlighting the need to maintain installed edge drains. Overall, for these two cases, only 15% of the simulations resulted in S_w values for the upper layer dropping below 10% by the 96th hour. The wide variance in the final S_w values for the cases with either no edge drain or a fouled edge drain requires further analysis to determine the source (i.e., the surface layer, the aggregate subbase, and the subgrade soil).

Grouping the data by either surface type (asphalt vs. concrete) or aggregate type (chert vs. limestone) provided no clarity. These groupings' final average Sw values ranged between 23% and 30%. In the simulations where PCC (Portland Cement Concrete) was used as the surface layer, the upper layer reached residual values within 49 hours. This was a faster response than that observed in the simulations using asphalt surface layers. The T_d values to the residual

moisture content for the asphalt simulations were greater than 50 hours. Regarding the different aggregate types, there was no difference (T-test; p = 0.54) in T_d to the residual moisture content between the pavement systems using either chert or limestone. However, the percent errors for each group were more important, which were greater than 50%, meaning that the variances were considerable.

Grouping the data by subgrade soil type showed significant differences (Figure 4-8; ANOVA; p < 0.001). The average final S_w values for the cases with a silt loam subgrade was 45% ± 5%. It took 83 ± 10 hr for the S_w of the upper layer to reach 50%. Silt loam soils have the slowest K_s of all soil types (e.g., Table 4-1), and K_s is a sensitive term in the drainage calculator (Papanicolaou et al., 2015b). The average final S_w for simulations using a silty clay loam subgrade was 20% ± 5%. In comparison, it took 40 ± 6 hr for the upper layer to reach an S_w of 50%. Finally, the scenarios with the loam subgrades drained the fastest, and the S_w of the upper layers reached 50% in 30 ± 5 hr, with an average final S_w value of 12% ± 4%.

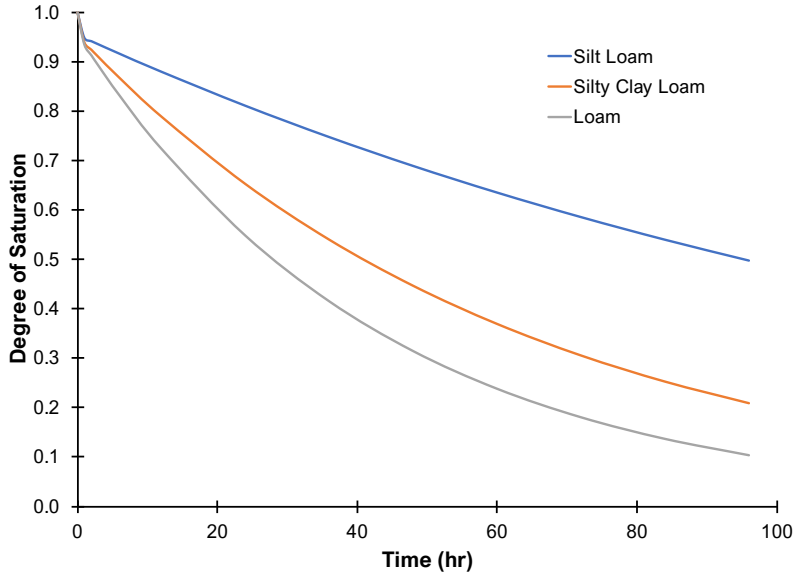

Figure 4-8. The change in the degree of saturation over a 96-hour simulation for three different subgrade soils: Silt loam; Silty clay loam; and Loam.

The soil type was the most influential characteristic, rather than the presence of a clean edge drain, that controlled the T_d values. One concerning aspect of pavement integrity, though, is that silt loam soils cover over 60% of the state. It takes approximately 3.5 days for the upper pavement-aggregate layer to drain to a saturation level of at least 50%.

4.3.2 Discussion on pavement bearing capacity

The pavement-aggregate-soil system also controls the pavement's bearing capacity and service life. The modulus of the materials has an important role in determining the total capacity. The modulus of the asphalt surface does not see significant changes in water content if it does not have any water-related damage. The modulus varies with moisture for the aggregate base and subgrade soil. This variation is expressed with different equations.

For aggregates, crushed stone like the Tennessee aggregate material was tested by Rada and Witczak (1981) at saturation levels of 65% and 85%. The 65% level was considered the normal

condition, while the 85% level was considered wet. The relationship between the modulus and stress as a function of moisture content is shown in the following K- θ equation:

$$M_R = K_1\theta^{K_2} \quad (4\text{-}1)$$

here $\theta = \sigma_1 + \sigma_2 + \sigma_3$ and is the bulk stress; K_1 and K_2 are moisture-related fitting parameters.

The soil resilient modulus has the following moisture-related expression from Uzan (1992):

$$M_R = K_3\theta^{K_4}\tau_{oct}^{K_5} \quad (4\text{-}2)$$

Where $\tau_{oct} = \sqrt{\frac{1}{3}[(\sigma_1 - \sigma_2)^2 + (\sigma_2 - \sigma_3)^2 + (\sigma_3 - \sigma_1)^2]}$ and is the octahedral shear stress, while K_3, K_4, and K_5 are moisture-dependent parameters. In Zuo et al. (2007), the normal saturation is 87%, and the wet saturation level is 92%. The resilient modulus parameters for the base materials are in Table 4-2, while the resilient modulus for the soil are in Table 4-3.

Table 4-1. Values of resilient modulus parameters for the base material (Zuo et al., 2007).

	Nominal (S=60%)	Wet (S=85%)
K_1 (psi)	6000	3500
K_1 (kPa)	495.2	49.6
K_2 (-)	0.5	0.7

Table 4-2. Values of resilient modulus parameters for subgrade material (Zuo et al., 2007).

	Nominal (S=87.4%)	Wet (S=92.3%)
K_3 (MPa)	6000	3500
K_4 (-)	495.2	49.6
K_5 (-)	0.5	0.7

Pavement capacity is determined by combining the modulus values of every layer. The modulus of asphalt surface is primarily influenced by temperature, and Zuo et al. (2007) found that moisture's effect on Tennessee pavements differs monthly because of the temperature variation. For example, the temperature is colder in March, and the asphalt is stiffer. The stress transferred into the unbound layers is low when the asphalt is stiffer. In the warmer month of May, the load is distributed deeper into the subgrade so that the capacity of the pavement is less. Therefore, the capacity of pavement relies not only on drainage and moisture but also on other environmental factors such as temperature.

4.4 Influence of Pavement Materials and Structures on Drainage

4.4.1 Model verification

The influences of pavement material and structure on drainage were studied with the ABAQUS simulations. The model was verified by simulating a pavement drainage system recorded in the literature (Hassan and White, 1996). The pavement section has a length of 220 cm, and vertically it has a surface layer, stabilized base, filter, and subgrade. The basic parameters of each layer in the simulation are shown in Table 4-4. The sorption characteristics of the material for each layer are shown in Table 4-5. The simulated rainfall event for the simulation is shown in Table 4-6.

Table 4-4. Thickness and basic properties of each layer.

Layer	Thickness (cm)	Density (g/cm^3)	Permeability (cm/s)
#11 surface	2.5	2.21	1.01e-4
#9 binder	3.8	1.995	1.11e-4
#8 binder	3.8	2.21	1.34e-4
#5C base	30.4	1.96	0.112797
#53 Coarse Agg.	21.6	2.30	0.035573
Subgrade Soil	30.0	2.7	7.73e-8

Table 4-5. Sorption characteristics of each material (pressure vs. volumetric water content).

Material	Pressure (bars)							
	0	*0.1*	*0.33*	*0.67*	*1.0*	*3.0*	*5.0*	*15*
#11 surface	0.016	0.013	0.0125	0.0125	0.0125	0.0125	0.0125	0.0125
#9 binder	0.055	0.024	0.024	0.024	0.024	0.024	0.024	0.024
#8 binder	0.031	0.015	0.015	0.014	0.014	0.014	0.014	0.014
#5C base	0.164	0.006	0.005	0.0039	0.003	0.002	0.002	0.002
#53 Coarse Agg.	0.279	0.087	0.074	0.053	0.046	0.03	0.290	0.020
Subgrade Soil	0.39	0.33	0.324	0.318	0.312	0.159	0.05	0.048

Table 4-6. Rainfall intensity vs. time

Time (hr)	Rainfall intensity (cm/hr)
1.75	0.114
2.75	0.2794
3.75	0.6096
4.75	0.2921
5.75	0.3048
6.75	0.01
7	0
8	0
9	0

The simulation results (Figure 4-9) showed satisfactory agreement with the measured data. The simulated peak velocity was close to that of the measured value, as was the trend of the falling limb of the hydrograph. The only exception was that the simulated velocity goes to 0 after 30 hr, while with the measured velocity, a small residual endured. By integrating under the hydrograph curve, the simulated total water flow was 3146 Liters, accounting for 89.3% of the measured value of 3521 Liters. Furthermore, from the comparison of saturation data before the rainfall (Figure 4-10), the simulated saturation levels of the base and subgrade agreed well with the measured data. The degree of saturation for the filter showed some differences with the gradual change from base to subgrade in the simulation results. The continuity requirement of FEM computation might cause the discrepancy. In general, the simulation method can be considered capable of simulating the real drainage process of pavement.

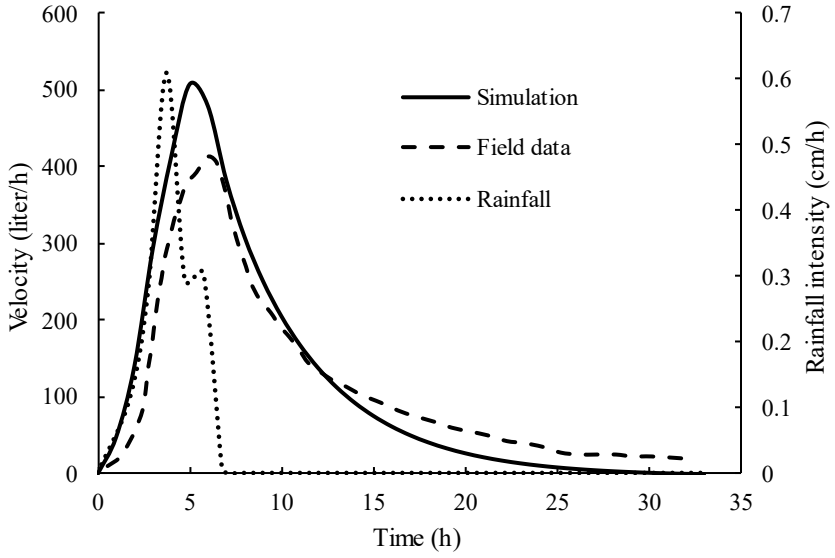

Figure 4-9. Verification results comparison of simulated and measured data.

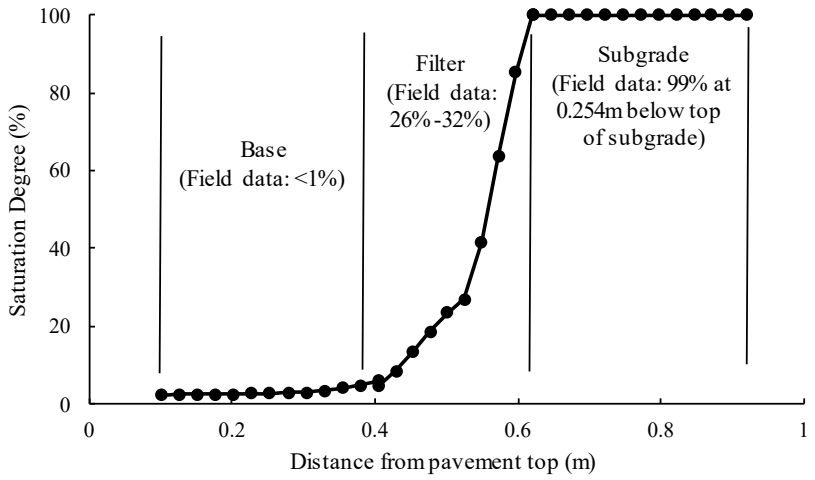

Figure 4-10. Comparison of saturation results for the simulated and measured data.

4.4.2 Influence of base and soil permeability combinations

The saturation level of the pavement was influenced by the permeabilities of the aggregate and the soil. Larger permeability led to higher drainability. Figure 4-11(a) shows the pavement degree of saturation after 2 hr draining from full saturation using a K_{base} = 1 m/hr and a K_{soil} = 0.001 m/hr. For this case, the bottom of the shoulder aggregate was still saturated, as was the base towards the pavement centerline. The permeabilities in Figure 4-11(b) are larger with K_{base} = 20 m/hr and a K_{soil} = 0.002 m/hr, which caused the pavement to drain quicker.

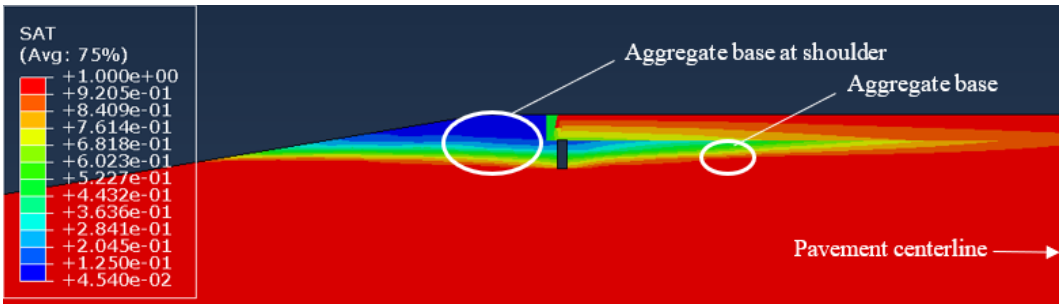

(a) Saturation distribution of pavement at K_{base} = 1 m/hr, K_{soil} = 0.001 m/hr.

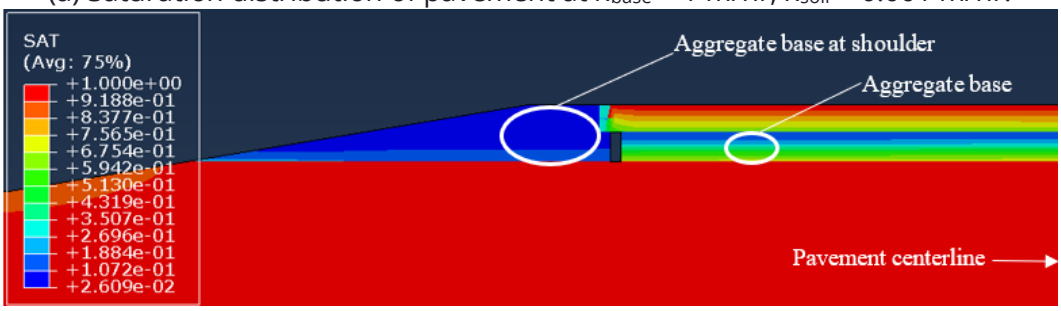

(b) Saturation of pavement at K_{base} = 20 m/hr, K_{soil} = 0.002 m/hr.

Figure 4-11. Comparison of saturation with different base/soil permeabilities.

For further analysis, the AASHTO drainage criteria for interstate highways was adopted as the index to evaluate the drainability of the whole pavement. The criteria states that T_d from 100% to 50% should be under 2 hr (FHWA, 1994; AASHTO, 1993). Additionally, the saturation level at the base layer's mid-depth was used to represent the saturation of the whole layer. Under different combinations of base & soil permeabilities, the saturation levels of the base layer at the pavement shoulder and the centerline are shown in Figures 4-12(a) and 4-12(b), respectively. Different colors represented saturation level in Figure 4-12: red is 75% to 100%, yellow is 50% to 75%, green is 25% to 50%, and blue is 0% to 25%. In Figure 4-12(a), the pavement shoulder drains well under all base/soil permeability combinations as the saturation level is always below 25%. The saturation level is low because the shoulder is close to the side drain, so water is effectively drained. In Figure 4-12(b), at the pavement centerline, the saturation remained higher than that at the shoulder because of the long path for water to reach the drainpipe. At low permeabilities of either the base or the soil, the saturation was higher than 50% and, hence, considered unsatisfactory.

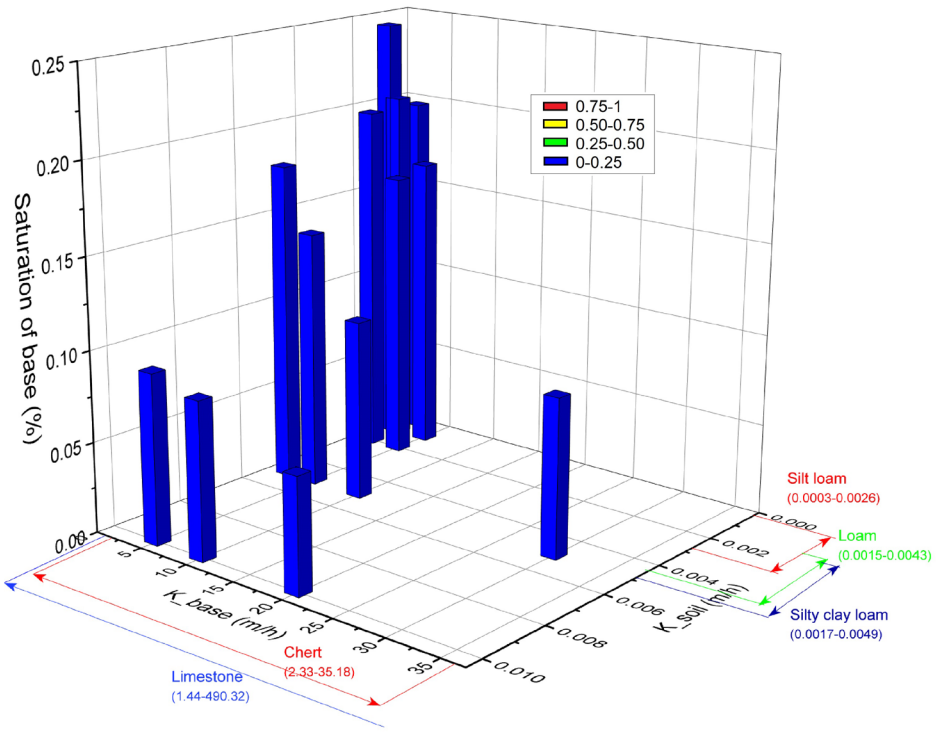

(a) Saturation of the base at pavement shoulder.

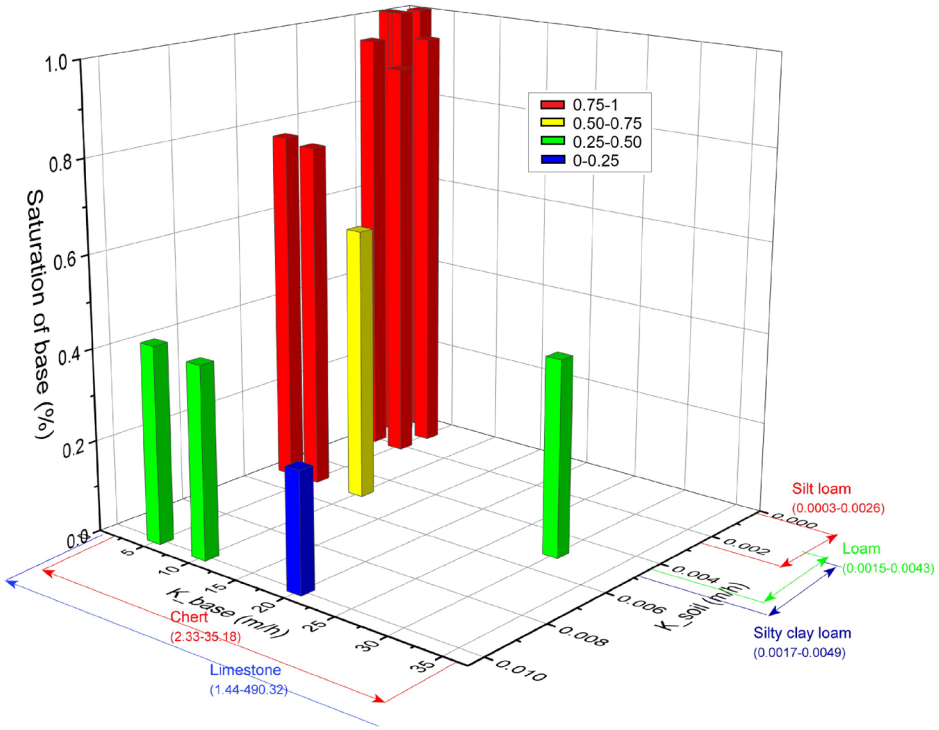

(b) Saturation of the base at pavement centerline.

Figure 4-12. Saturation of base aggregate under base/soil permeability combinations.

The relationship between S_{base}, K_{base}, and K_{soil} is very strong. The following relationship was obtained from a multiple linear regression using data in Figure 4-12:

$$S_{base} = 1.0655 - 0.0126 \times K_{base} - 55.0707 \times K_{soil} \qquad (R^2 = 0.99) \qquad (4\text{-}3)$$

The significance values of Equation (4-3) were determined using an F-test and are in Table 4-7. The results show that the coefficients in Equation 4-3 are significant and that K_{soil} is more influential than K_{base}.

Table 4-7. ANOVA of multiple linear regression of Equation 4-3.

	DF	Sum of squares	Mean square	F value	p-value
Model	2	0.8539	0.4270	528.82	7.208E-11
Error	10	0.00807	8.073E-4		
Total	12	0.8620			

Four special cases were used with Equation 4-3 (Table 4-8). The special cases use the threshold of S_{base} being less than or equal to 50%. The cases show that if K_{base} is large enough, as with high-quality limestone (i.e., greater than 44 m/hr), the choice of soil is unrestricted (Case 1). Yet, if K_{base} is too small, the drainability cannot be satisfactory, regardless of the soil type used (case 2). When K_{soil} is too small (e.g., less than 0.00225 m/hr), chert is not recommended as the base material because of its low permeability (case 3). Case 4 shows that the minimum value for K_{base} is 23.54 m/hr for satisfactory drainability.

Table 4-8. Special cases calculated by Equation 4-3.

Special Case	K_{base}	K_{soil}	S_{base}
1	43.71	0.0003	50%
2	1.44	0.0049	77.8%
3	35.18	0.00225	50%
4	23.54	0.0049	50%

4.4.3 Influence of surface parameters

The influence of surface permeability is shown in Figure 4-13. Under a fixed K_{base}/K_{soil} combination (5/0.005m/h), the permeability of the asphalt layer was in the range of most commonly used surface materials. Still, the results show very limited variation for S_{base}. Regardless of $K_{surface}$, the degree of saturation in the base remained nearly constant at 75%. The conclusion can be drawn that the effect of surface permeability on base saturation is very limited and could be neglected.

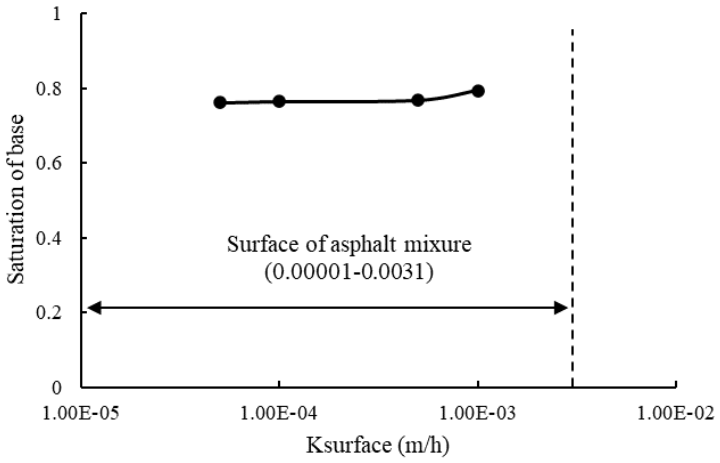

Figure 4-13. Influence of surface permeability.

4.4.4 The effects of roadway dimensions on drainability

The influences of base layer thickness, pavement width, and base slope were also examined in Figures 4-14, 4-15, and 4-16, respectively. Base layer thickness and pavement width both had quantifiable influences on S_{base}. The thicker bases resulted in lower degrees of base saturation. Greater pavement width increased the travel length for water to reach the drainage pipe so that the base saturation increased. Additionally, higher base slopes resulted in less water remaining in the aggregate. The drainage design should also consider the influence of pavement width and base layer thickness when using Equation 4-3. The comprehensive consideration of materials and pavement dimensions will be addressed in section 4.6.

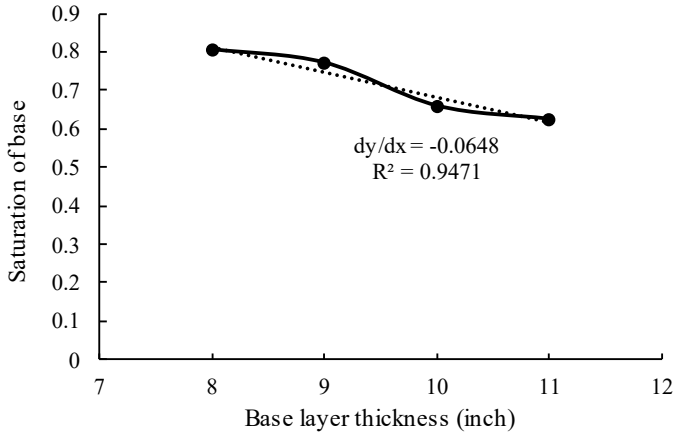

Figure 4-14. Influence of base layer thickness.

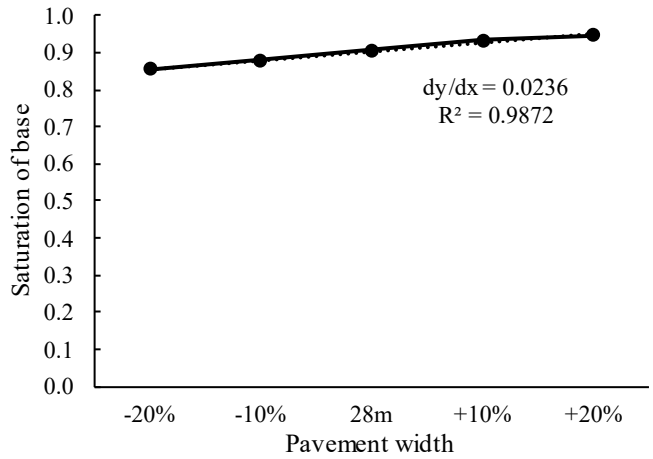

Figure 4-15. Influence of pavement width.

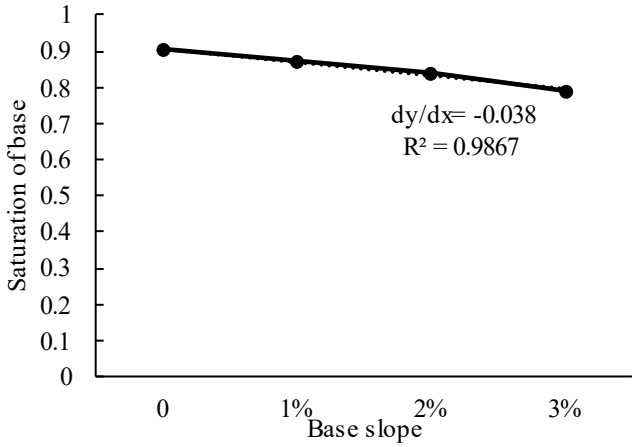

Figure 4-16. Influence of base slope.

4.4.5 Effect of rainfall on saturation of pavement layers

Initially, the whole pavement structure was saturated and allowed to drain for 24 hours. After 24 hours of drainage, the base saturation was near its residual water content (Figure 4-17(a)). With the rainfall, the base saturation of the shoulder increased with the additional influx of water (Figure 4-17(b)). However, the base saturation of the main part of the roadway did not increase with the rainfall because an asphalt layer protected it. The base saturation at the pavement centerline and the soil below (Figure 4-18) even showed a slight decrease, indicating that it is not affected by the rain.

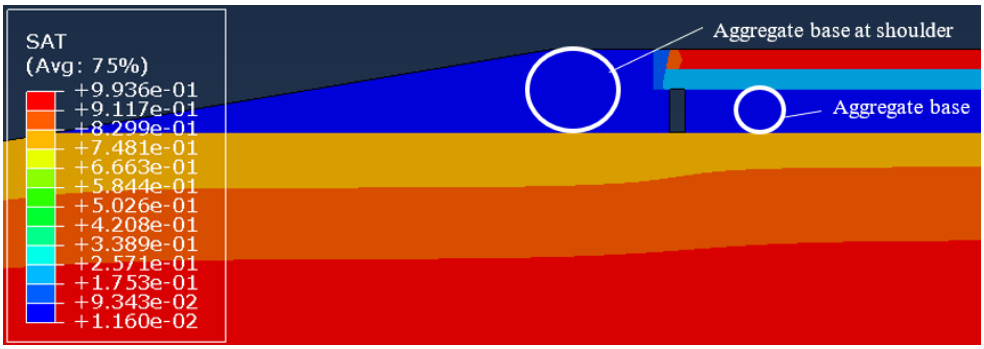

(a) Saturation of pavement before the rainfall (time = 24 hr).

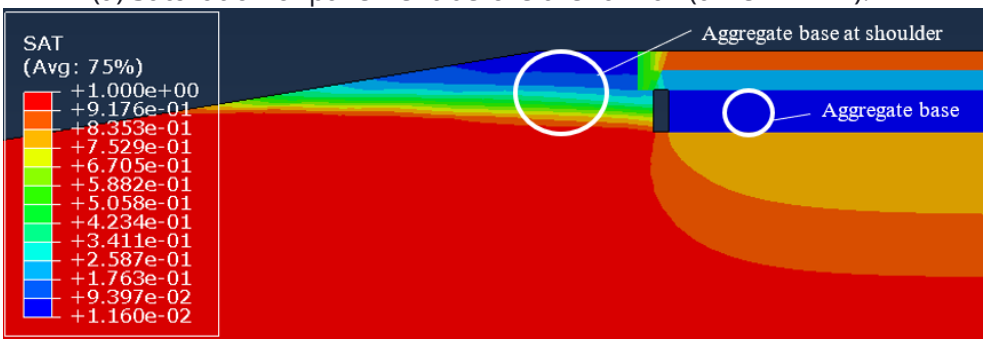

(b) Saturation of pavement during the rainfall (time = 48 hr).

Figure 4-17. Saturation of the pavement before and during the rainfall.

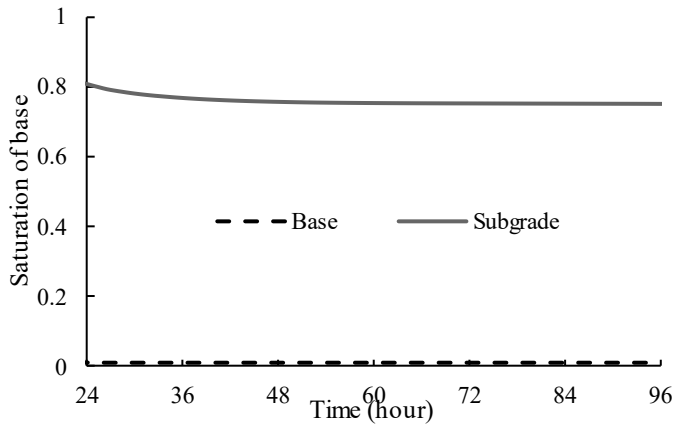

Figure 4-18. Saturation of the base at pavement centerline during the rainfall.

Moreover, the saturation level of the aggregate base under the pavement remained under 10% even when $K_{surface}$ was given a value that surpassed the maximum value found in the literature, 3.1 X $10^{\wedge-3}$ m/hr (Figure 4-19). It should be noted that the base at the centerline is right beneath the crack. This means that a single crack in the pavement has very limited influence on pavement saturation. Concrete pavement has even smaller surface permeability (Liu, 2005). Therefore, the base saturation at the centerline for concrete pavement should be even lower.

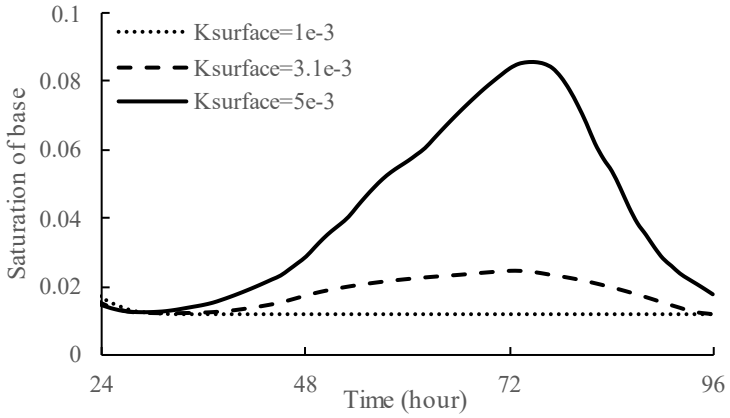

Figure 4-19. Influence of $K_{surface}$ on base saturation at the pavement centerline during the rainfall.

During a rain event, the water enters the pavement mainly through the shoulder, yet the pavement is still draining simultaneously. The first consideration for drainage during rainfall is that if water enters fast enough to exceed its drainage capacity, water will accumulate on the pavement. The second consideration is that the pavement drainage is considered unacceptable if the saturation of pavement is too high because the capacity of the pavement is lowered, and water damage to materials may occur. With limited support in the literature for a certain level of saturation that should be considered an acceptable threshold, the value of 50% was chosen following AASHTO saturation criteria which seems reasonable, meaning the saturation should always be kept under 50% saturated in heavy rainfall. Unlike the analysis in 4.3.2, this analysis will focus on the should because the rainfall had very little effect on the base and soil saturation values below the paved sections of the road. Here the center of the base at the shoulder is used to represent the saturation of the base because the surface well protects the base at the centerline.

Figure 4-20 shows that the base saturation increased slowly and rapidly when the rainfall started at time = 24 hr. Under different combinations of the base/soil permeabilities, the maximum saturation level of the base ranged from 50% to 100% (Figure 4-20). It should be reiterated that from time = 0 hr to time = 24 hr, the pavement-aggregate-soil structure has been draining, and at this time, the pavement is assumed to have reached an equilibrium condition.

To develop a relationship for the maximum saturation level (represented by S_{base1}) based on the permeability of base and soil, several simulations were conducted, and the results are shown in Figure 4-21. Equation 4-4 was obtained through multiple linear regression. Although the coefficient of determination was only 0.67, an ANOVA showed the relationship was still significant (Table 4-9).

$$S_{base1} = 0.9062 - 0.0102 \times K_{base} - 10.7050 \times K_{soil} \qquad (R^2 = 0.67) \qquad (4\text{-}4)$$

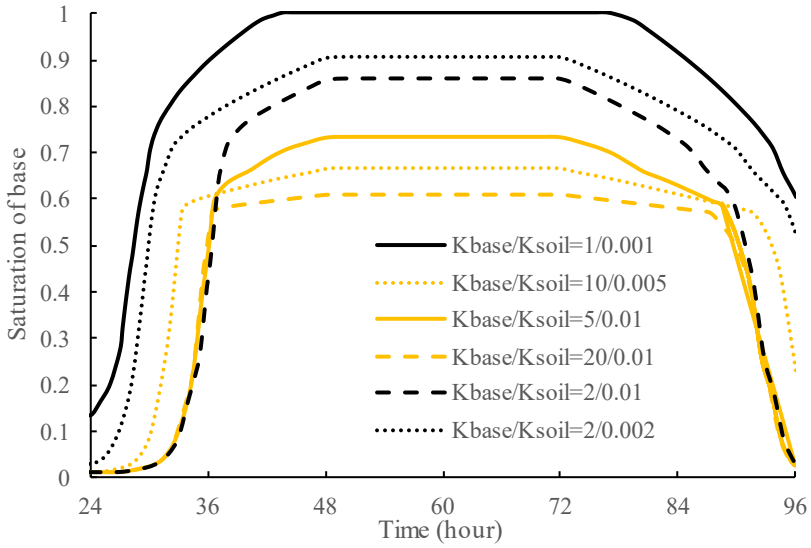

Figure 4-20. Saturation of base under rainfall.

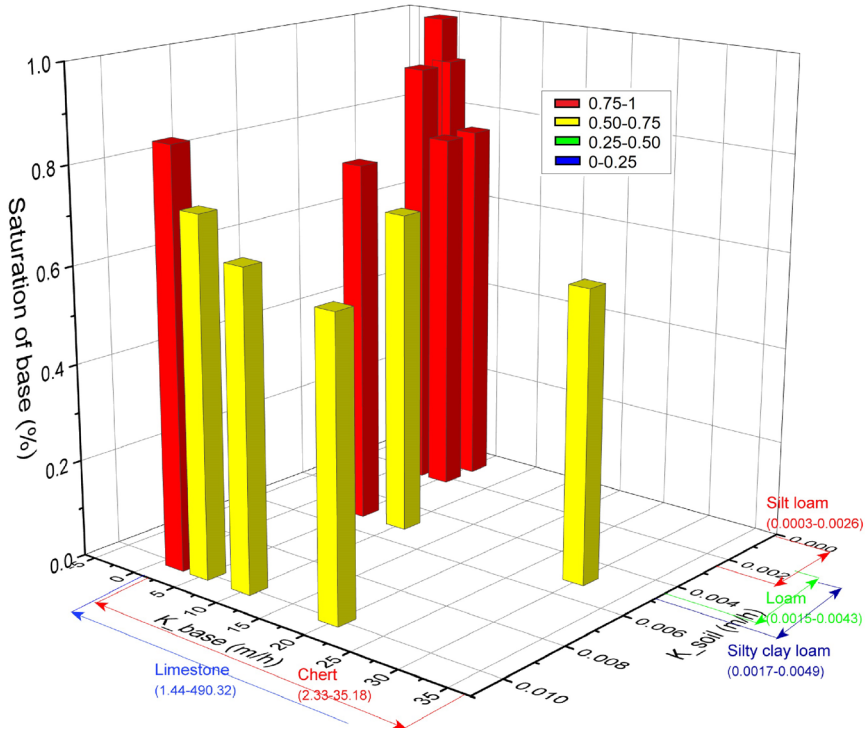

Figure 4-21. Maximum saturation of the base (S_{base1}) at shoulder under K_{base}/ K_{soil} combinations.

Table 4-9. ANOVA of multiple linear regression of Equation 4-4.

	DF	Sum of squares	Mean square	F value	Prob>F
Model	2	0.1306	0.0653	12.2346	0.0027
Error	9	0.0480	0.0053		
Total	11	0.1787			

Equation 4-4 shows that K_{soil} also plays a more important role in maximum saturation level than K_{base}. However, a comparison of Equations 4-3 and 4-4 shows that K_{soil} during rainfall becomes less critical. This is because water mainly permeates through the pavement shoulder, and a larger K_{base} allows water to permeate faster. With the equation 4-4, it is known that heavy rainfall usually does not fill the base layer to full saturation for the common base and subgrade materials.

Additionally, there are special cases shown in Table 4-10. When K_{soil} is too small (e.g., 0.0003 m/hr), chert is not recommended as the base material because of its low permeability (case 1). However, the base material is also important because pavement cannot rely on good soil solely to obtain satisfactory drainage (case 2). If K_{base} is too small, the pavement can be highly saturated even if the soil is very good (case 3); if K_{base} is large enough (e.g., greater than 89 m/hr), the pavement will not be filled with water at all during rainfall (cases 4 and 5).

Table 4-10. Special cases calculated by Equation 4-4.

Special Case	K_{base} (m/hr)	K_{soil} (m/hr)	S_{base1}
1	35.18	0.0003	0.544
2	34.68	0.0049	0.5
3	1.44	0.0049	0.839
4	88.6	0.0003	0
5	83.7	0.0049	0

Pavement base layer thickness has negligible influence on S_{base1} during the rainfall, as seen in Figure 4-22.

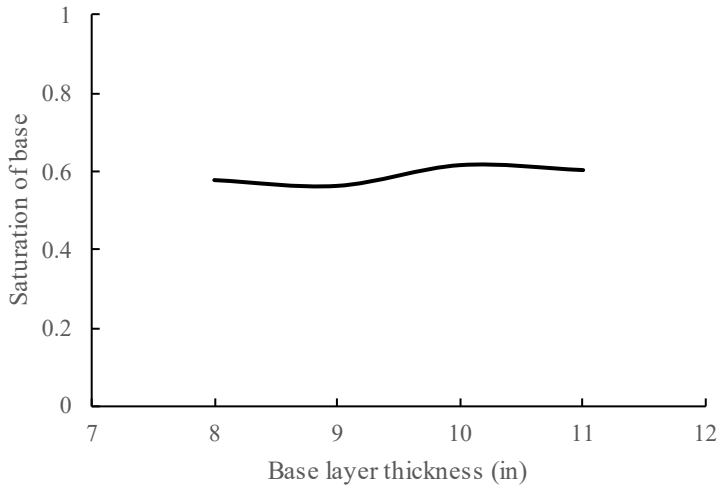

Figure 4-22. Influence of base layer thickness.

4.5 Laboratory Test Results and Discussion

The test results after draining from an initial state of 100% saturation. Data were collected for 2 hours following the 2-hour draining criterion. The results are shown in Figures 4-23 and 4-24. In the figures, the S and A refer to soil and aggregate; 1 and 2 refer to a different locations (shown in Figure 3-5).

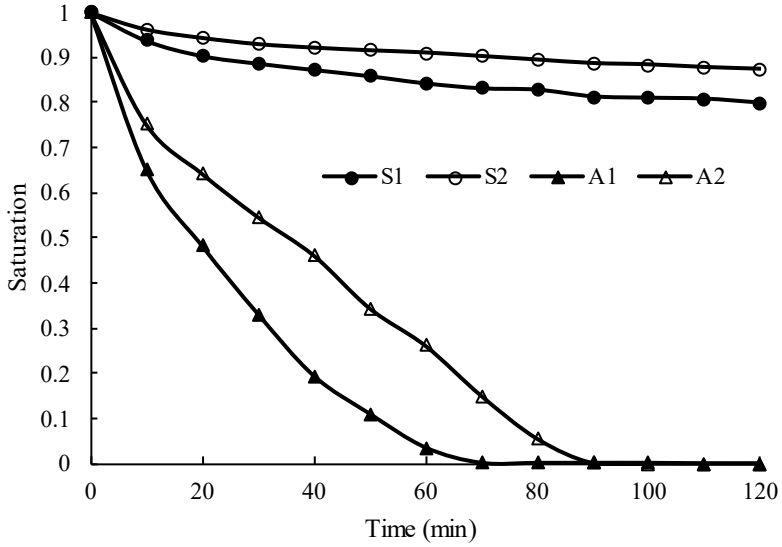

Figure 4-23. Saturation vs. time, Limestone/silt loam as base/subgrade (shoulder).

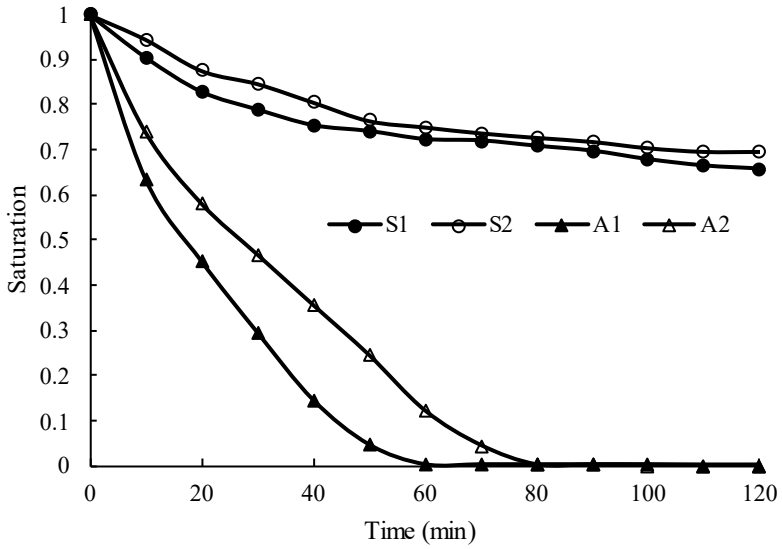

Figure 4-24. Saturation vs. time, Limestone/loam as base/subgrade (shoulder).

From Figures 4-23 and 4-24, soil saturation remains high at the shoulder, but the saturation of loam has lower saturation because of its high drainability. The side drain works well at the shoulder, so the shoulder drains quickly close to the residual saturation in about an hour. Looking at the A1 curve in Figures 4-23 and 4-24, soil drainability affects the shoulder drainage by shortening drainage time by about 10 mins (from 70min to 60min).

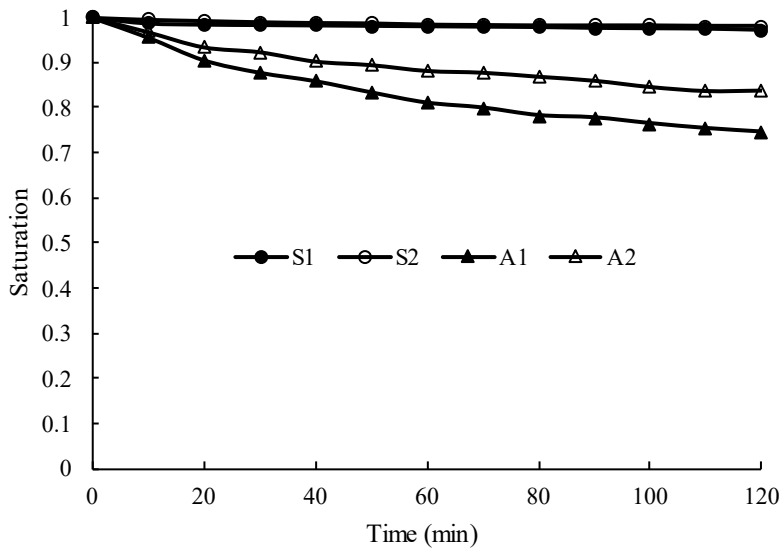

Figure 4-25. Saturation vs. time, Limestone/silt loam as base/subgrade (middle).

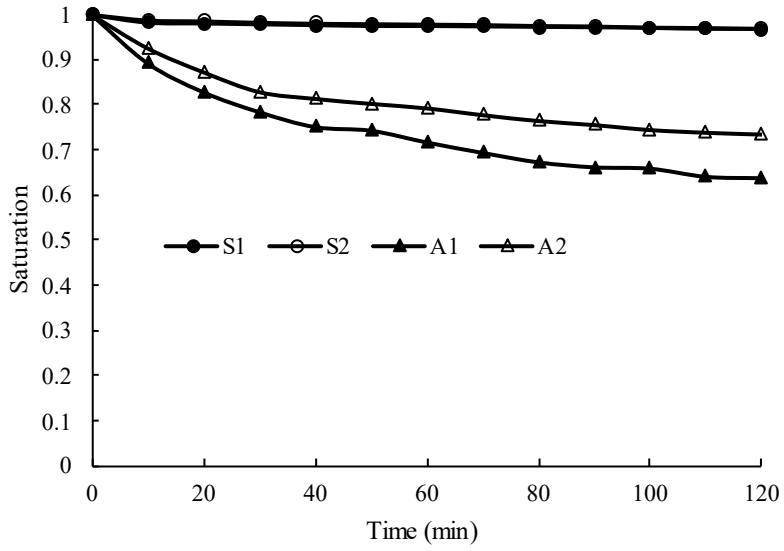

Figure 4-26. Saturation vs. time, Limestone/loam as base/subgrade (middle).

Additionally, Figures 4-25 and 4-26 show that soil saturation remains close to 100% in the middle of the pavement. The drainability of soil affects the middle drainage by lowering saturation by about 10.6%. The experiment simulation of middle pavement is under the extreme hypothesis that water cannot drain through the drainpipe. The actual effect of soil on saturation is less than 10.6%.

4.6 Nomograph and Design Recommendations

4.6.1 Development of nomograph

Using Figures 4-14, 4-15, and 4-16, the difference between the S_{base} from a baseline simulation (h=0.254m, w=28m, s=0) is expressed with a deviation index d, calculated by

$$d = \left(\frac{h - 0.254}{0.0254}\right) \times 0.0648 - \left(\frac{w - 28}{28 \times 0.1}\right) \times 0.0236 + 3.8s$$

$$d = 2.551h - 8.43 \times 10^{-3}w + 3.8s - 0.412 \quad (4\text{-}5)$$

where d is the S_{base} deviation index; h is the depth is base (m); w is the width of pavement (shoulder to shoulder distance, m); s is the slope of the base layer.

A nomograph can be developed combining Equations 4-3 and 4-5 (Figure 4-27). The nomograph can be used to determine K_{base} with K_{soil}.

From Equation 4-4, a single line is added in Figure 4-27 (the dashed line). However, this line is obtained under the premise of heavy rainfall. If the precipitation in the region where the pavement is located is relatively low, this criterion can be less stringent. For Region 4, where precipitation is highest, it is recommended to avoid chert and use limestone as the base material.

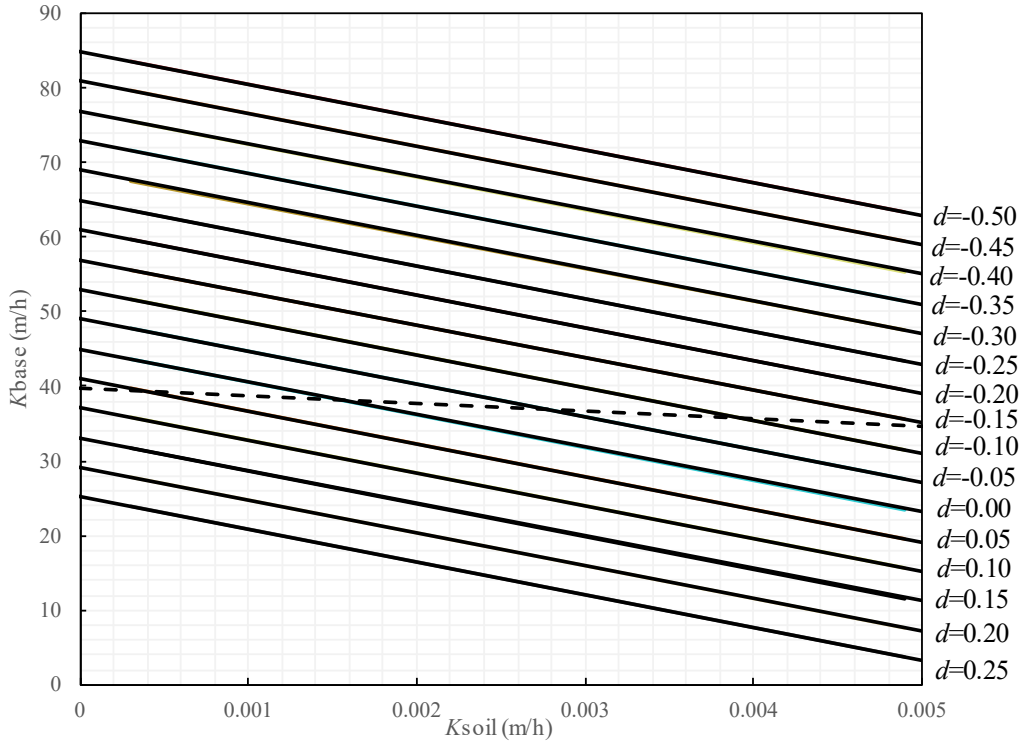

Figure 4-27. Nomograph to determine K_{base} with K_{soil} (ensure 50% drainage in 2 hr).

4.6.2 Example of using the nomograph

The following is an example of using the developed nomograph to check the compatibility of base and subgrade materials and pavement structural characteristics to ensure drainability.

Figure 4-28 is a typical cross-section of I-40, consisting of asphalt surface layers, base, and subgrade. The pavement dimensions are assumed as follows: the thickness of base h = 0.264 m, pavement width w = 34.1 m, base slope s = 0.02. Materials hydraulic conductivity are: K_{base} = 55 m/hr, K_{soil} = 0.0015 m/hr.

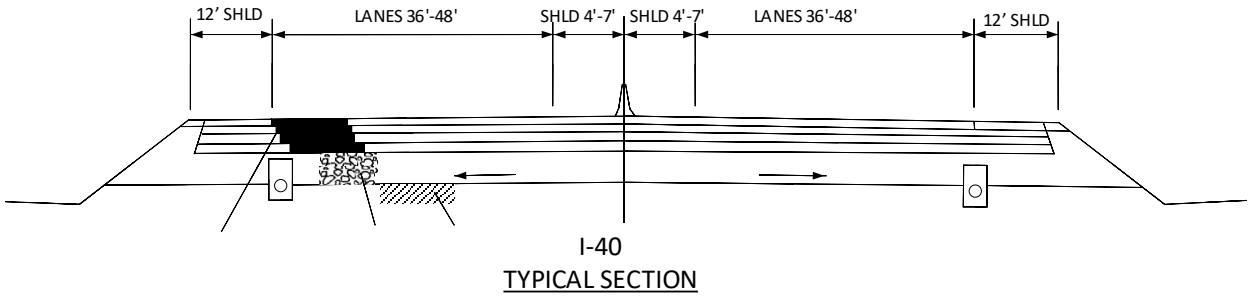

Figure 4-28. Typical section of pavement used as an example.

Calculation & analysis:

1) Calculate Equation 4-5.
2) Identify the solid line with d=0.05 on the nomograph. The identified solid line is colored in red, as shown in Figure 4-29.
3) Draw K_{base}/K_{soil} point on the nomograph with K_{base} = 55 m/hr and K_{soil} = 0.0015 m/hr. The point is above the red and dashed lines, as shown in Figure 4-29.
4) The conclusion can be drawn that the proposed drainage design can satisfy the 2-hr saturation down 50% criterion. The aggregate base layer will not be saturated over 50% during heavy rainfall.

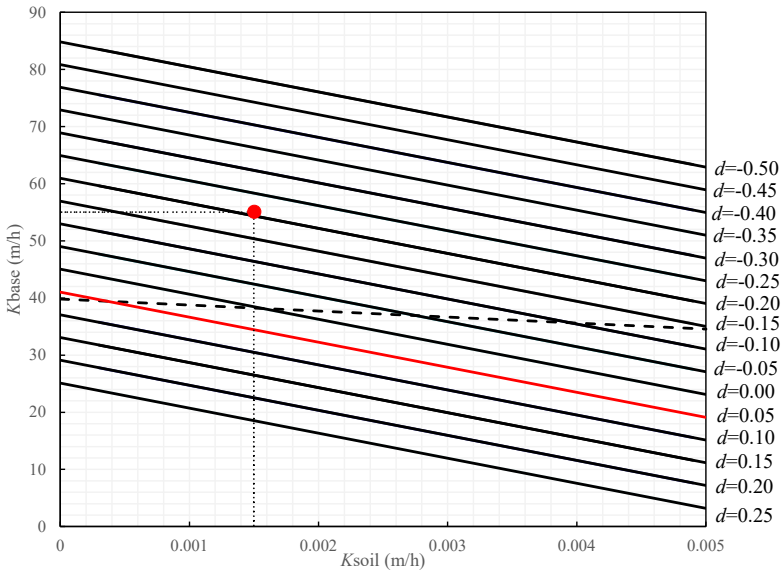

Figure 4-29. Example of using the nomograph.

4.7 Flow Chart of Assessment

The pavement subsurface drainage assessment is recommended to be carried out by the flow chart shown in Figure 4-30.

The pavement subsurface drainage assessment should be implemented under three categories. The first category is the quantitative assessment, which involves the usage of nomographs. Pavement dimensions are used to calculate deviation index *d*, and material hydraulic conductivities are located on the nomograph for comparison. The second category is the qualitative assessment, which involves the consideration of pavement drainage history correlated to pavement location. The third category is abnormity examination. The drainage pipe clog is the main abnormality that significantly undermines the pavement's drainage ability.

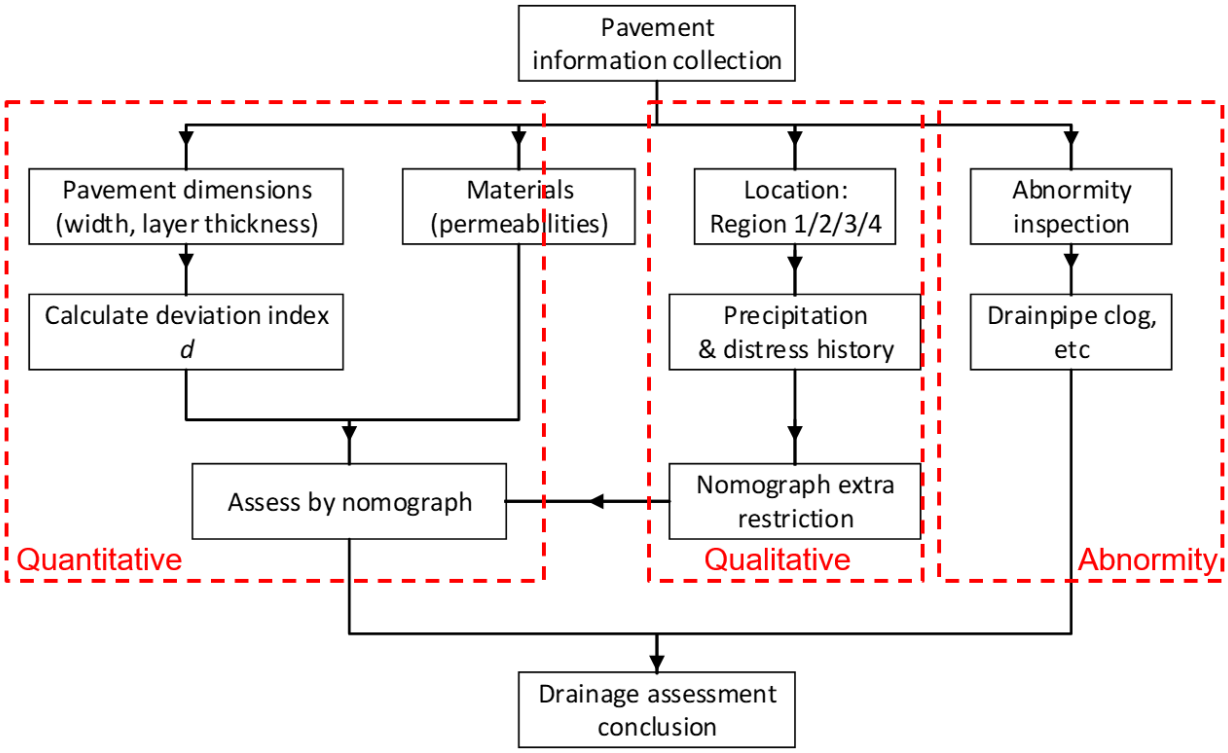

Figure 4-30. Flow chart of pavement subsurface drainage assessment.

Chapter 5 Conclusion

This project investigated the factors influencing roadway subsurface drainage and proposed a method to evaluate roadway subsurface drainage practices. The project focuses on the hydraulic parameters that can cause insufficient drainage systems. An investigation starts with a database analysis to draw a map of soil and pavement conditions and study the correlation between soil hydraulic conductivity and pavement roughness. A drainage calculator was developed to assess the performance of different drainage designs. To consider more influencing factors of pavement drainage, a full-scale pavement drainage simulation was carried out, and the influence of the factors were quantified. Furthermore, a nomograph was developed by integrating influencing factors in one equation. The nomograph can be employed in supporting pavement drainage design and assessment.

This project showed that most of the pavement sections in Tennessee are in "Good" condition in terms of moisture-related distress. Those sections rated as "Poor" are mainly located in west Tennessee, with only a few weak spots in east Tennessee.

For the roadways classified as "Poor," the subgrade soil was the most important characteristic influencing pavement drainability. The influence of the subgrade soil outweighed the influences of the pavement surface and aggregate types. This finding was supported by a database analysis showing how soil drainability correlated with pavement condition. Soil drainability was more influential than high precipitation and shallow water tables.

Finite Element Method simulations of the whole pavement-aggregate-soil structure showed that pavement drainability is influenced by the combination of base and subgrade material, as well as pavement dimensions, such as aggregate base thickness, pavement width, and base slope. The influence of these factors can be quantified and integrated into one equation.

The most vulnerable part of pavement during rainfall is the shoulder because the middle part of pavement is protected by surface structure. Rainfall entering through cracks or joints had limited effects on saturation levels. The saturation of pavement during rainfall is influenced by base/subgrade hydraulic conductivity but not significantly influenced by pavement dimension factors.

The **benefits of this project** included a proposed method to evaluate roadway subsurface drainage practices. The **deliverables** are a nomograph and a flow chart that provide a quantitative way to evaluate pavement drainage capability considering the aggregate and in-situ soil material properties and the pavement dimensions. **Recommendations** for material properties include the following:

1) If K_{soil} is too small (e.g., less than 2.25 X 10^-3 m/hr), chert is not recommended as the base material because of its low permeability.
2) Aggregate base materials with a permeability large enough (e.g., larger than 44 m/hr) can be used with any subgrade soil type in Tennessee and still provide sufficient roadway drainage.
3) It is recommended to check the compatibility of base and subgrade materials and pavement structural characteristics using the nomograph to ensure the drainability of pavement.

4) For regions with greater precipitation and poor IRI history (especially for some areas of Region 4), more stringent criteria for drainage assessment is recommended to minimize the risk of drainage-related pavement distress.
5) A comprehensive assessment should be performed for any target pavement section, including quantitative assessment, qualitative assessment, and abnormity assessment.

Future research efforts may include a more comprehensive big data analysis considering other factors like pavement age and a simulation considering the other factors of pavement drainage such as temperature. Additionally, more understanding is needed to improve the 2-hour drainage criterion. Pavements usually do not get fully saturated even under heavy rain, so the initial saturation level of pavement should not be 100%. The 2-hour drainage criterion should be modified based on the real pavement saturation levels.

References

1. American Association of State Highway and Transportation Officials (AASHTO). 1993. *Guide for design of pavement structures*. Washington, D.C.
2. American Association of State Highway and Transportation Officials (AASHTO). 2009. *Rough roads ahead, fix them now or pay for it later*. Washington, D.C.
3. Aboufoul, M., and A. Garcia. 2017. Factors affecting hydraulic conductivity of asphalt mixture. *Materials and Structures*. 50:116. DOI 10.1617/s11527-016-0982-6.
4. Bhattacharya, B.B., M.P. Zola, S. Rao, K. Smith, and C. Hannenian. 2009. Performance of edge drains in concrete pavements in California. *Proceeding of the National Conference on Preservation, Repair and Rehabilitation of Concrete Pavements*. St. Louis, MO. April 22-24, 2009.
5. Brooks, R.H., and A.T. Corey. 1964. Hydraulic properties of porous media. *Colorado State University Hydrology Paper*. 3. 27 pp.
6. Christopher, B.R., C. Schwartz, and R. Boudreau. 2006. *Geotechnical aspects of pavements*. Federal Highway Administration – National Highway Institute Course No. 132040.
7. Christopher, B.R., and V.C. McGuffey. 1997. *Pavement subsurface drainage systems*. Synthesis of Highway Practice 239. Transportation Research Board, National Academy Press. Washington, D.C.
8. Daleiden, J.F. 1998. *Video inspection of highway edge drain system: Evaluation of edge drains*. Report FHWA-SA-98-044, Federal Highway Administration.
9. Elhakeem, M., A.N. Papanicolaou, C.G. Wilson, Y.-J. Chang, C.L. Burras, B.K.B. Abban, D.A. Wysocki, and S. Wills. 2018. Understanding saturated hydraulic conductivity under seasonal changes in climate and land use. *Geoderma*. 315:75-87.
10. Ellithy, G. 2017. *Spreadsheet for estimating Soil Water Characteristic Curves (SWCC)*. US Army Corps of Engineers. ERDC/GSL TN-17-1
11. Federal Highway Administration (FHWA). 1994. *Drainable pavement systems — Instructor's guide*. Publication No. FHWA-SA-94-062. Office of Technology Applications and Office of Engineering, Federal Highway Administration, Washington, DC.
12. Gupta, S., A. Singh, and A. Ranaivoson. 2004. *Moisture retention characteristics of base and sub-base materials*. Minnesota Department of Transportation. MN/RC – 2005-06.
13. Hassan, H.F., and T.D. White. 1996. *Locating the drainage layer for flexible pavements*. Purdue University/Indiana Department of Transportation JHRP; Indiana Department of Transportation; Federal Highway Administration, 284 p.
14. Hossam, H., T.D. White, R. McDaniel, and D. Andrewski. 1996. Indiana subdrainage experience and application. *Transport Research Record*. 1519.
15. Huang, Y.H. 2004. *Pavement Analysis and Design*. Pearson Prentice Hall.

16. Kuttah, D., and H. Arvidsson. 2017. Effect of groundwater table rising on the performance of a Swedish-designed gravel road. *Transportation Geotechnics*. 11:82-96.

17. Liu, Y. 2005. *Three-dimensional finite element modeling of pavement subsurface drainage systems*. University of Kentucky Doctoral Dissertations. 311.

18. Maidment, D.R. 1993. *Handbook of Hydrology*. McGraw-Hill, Inc.

19. Mays, L.W. 2005. *Water Resources Engineering*. Wiley & Sons, Inc.

20. Meyer, P.D., M.L. Rockhold, and G.W. Gee. 1997. *Uncertainty analyses of infiltration and subsurface flow and transport for SDMP sites*. NUREG/CR-6565. PNNL-11705. U.S. Nuclear Regulatory Commission. Washington, DC.

21. Moulton, L.K. 1980. *Highway subdrainge design*. Report No. FHWA-TS-80-224. Federal Highway Administration. Washington, D.C.

22. National Cooperative Highway Research Program (NCHRP). 2001. *Impact of new information and communication technologies on transportation agencies: A synthesis of highway practice*. NCHRP Synthesis 296. Transportation Research Board — National Research Council. National Academy Press. Washington, D.C. — 2001. 67 P.

23. Nhantumbo, A.B.J.C., and A.H. Cambule. 2006. Bulk density by Proctor test as a function of texture for agricultural soils in Maputo province of Mozambique. *Soil & Tillage Research*. 87:231–239.

24. Nokkaew, K. 2014. *Hydraulic properties of recycled pavement aggregates and effect of soil suction on resilient modulus for pavement design*. Dissertation. University of Wisconsin – Madison.

25. Norambuena-Contreras, J., E. Asanza Izquierdo, D. Castro-Fresno, M.N. Partl, and Á. Garcia. 2013. A new model on the hydraulic conductivity of asphalt mixtures. *International Journal of Pavement Research Technology*. 6(5):488-495

26. Pachepsky, Y.A., W.J. Rawls, and H.S. Lin. 2006 Hydropedology and pedotransfer functions. *Geoderma*. 131:308– 316.

27. Papanicolaou, A.N., M. Elhakeem, C.G. Wilson, C.L. Burras, L.T. West, H. Lin, B. Clark, and B.E. Oneal. 2015a. Spatial variability of saturated hydraulic conductivity at the hillslope scale: Understanding the role of land management and erosional effect. *Geoderma*. 243-244 (2015):58-68. DOI: 10.1016/j.geoderma.2014.12.010

28. Papanicolaou, A.N., F. Bressan, C.G. Wilson, and A.G. Tsakiris. 2015b. *Development of a subgrade drainage model for unpaved roads*. IIHR – Hydroscience & Engineering, Department of Civil & Environmental Engineering, University of Iowa. Final report no. TR-654; 2015.

29. Pease, R.E. 2010. *Hydraulic properties of asphalt concrete*. Dissertation. University of Minnesota.

30. Rada, G. and Witczak, M.W. 1981. Comprehensive evaluation of laboratory resilient moduli results for granular material. *Transportation Research Record*. 810. Transportation Research Board, Washing-ton, D.C., 23–33.

31. Rawls, W.J., D.L. Brakensiek, and K.E. Saxton. 1982. Estimation of soil water properties. *Transactions of the American Society of Agricultural Engineers*. 25(5):1316-1320.2

32. Schaap, M.G., P.J. Shouse, P.D. Meyer. 2003. *Laboratory measurements of the unsaturated hydraulic properties at the vadose zone transport field study site*. Report for the U.S. Department of Energy. DE-AC06-76RL01830.

33. Schaefer, V.R., L. Stevens, D.J. White, and H. Ceylan. 2008. *Design guide for improved quality of roadway subgrades and subbases*. Final Report, Iowa Highway Research Board Project TR-525, 132 pp.

34. Uzan, J. 1992. Resilient characterization of pavement materials. *Int. J. Numer. Analyt. Meth. Geomech.* 166:435–459.

35. Voller, V. 2003. *Designing Pavement Drainage Systems: The MnDRAIN Software*. Final Report MN/RC - 2003-17.

36. Wagner, L.E., N. M. Ambe, and D. Ding. 1994. Estimating a Proctor density curve from intrinsic soil properties. *Transactions of the ASAE*. 37(4):1121-1125.

37. Wang, H., B. Xiao, M. Wang, and M. Shao. 2013. Modeling the soil water retention curves of soil-gravel mixtures with regression method on the Loess Plateau of China. *PLoS ONE* 8(3): e59475. doi:10.1371/journal.pone.0059475

38. Wei, Y., Hansen, W., and Schlangen E. 2008. Moisture warping in slabs on grade. *Proceedings of the 6th Rilem International Conference on Cracking in Pavement*, Chicago, USA, 16-18 June 2008

39. White, D., H. Ceylan, C. Jahren, T.H. Phan, S.J. Kim, K. Gopalakrisnan, and M. Suleiman. 2008. *Performance evaluation of concrete pavement granular subbase-pavement surface condition evaluation*. Final Report, IHRB Project TR-554, CTRE Project 06-250.

40. White, D.J., P.K.R. Vennapusa, D. Eichner, H. Gieselman, L. Zhao, C. Jahren. 2009. *Rapid, self-contained in-situ permeameter for field QA/QC of pavement base/subbase materials.* Final Report for Highway IDEA Project 130. Transportation Research Board. Washington DC.

41. Wilson, C.G., A.N. Papanicolaou, B.K.B. Abban, V.B. Freudenberg, S.M. Ghaneeizad, C.P. Giannopoulos, and H.T. Hilafu. 2022. Comparing spatial and temporal variability of the system water use efficiency in a Lower Mississippi River Watershed. *Journal of Hydrology – Regional Studies*. In Press.

42. Wilson, C.G. 2021. *Performance base testing for Erosion Prevention and Sediment Control (EPSC) devices*. A final report to Tennessee Department of Transportation. Nashville, TN.

43. Wosten, J.H.M., A. Lilly, A. Nemes, C. Le Bas. 1999. Development and use of a database of hydraulic properties of European soils. *Geoderma*. 90:169–185.

44. Zuo, G., E.C. Drumm, and R.W. Meier. 2007. Environmental effects on the predicted service life of flexible pavements. *Journal of Transportation Engineering*. 133(1):47-56.

Appendices

Table A1. Configurations of the upper layer in the drainage calculator simulations.

Scenario (Depth in cm)	PCC	D	BM2	A	A/S	Chert	Limestone	Total
1	0	3.175	5.08	15.24	0	25.4	0	49
2	0	3.175	5.08	15.24	0	0	25.4	49
3	0	3.175	5.08	7.62	7.62	25.4	0	49
4	0	3.175	5.08	7.62	7.62	0	25.4	49
5	25.4	0	5.08	0	0	25.4	0	56
6	25.4	0	5.08	0	0	0	25.4	56
7	25.4	0	0	0	15.24	25.4	0	66
8	25.4	0	0	0	15.24	0	25.4	66

Table A2. Degree of Saturation at different hours of the simulations. Saturation of Surface-Aggregate Layer by Hour

Scenario	0	1	2	3	6	12	24	36	48	60	72	84	96
1-N-SL	1.00	0.97	0.96	0.95	0.92	0.87	0.76	0.67	0.59	0.52	0.46	0.41	0.36
1-N-SCL	1.00	0.96	0.94	0.92	0.86	0.75	0.57	0.44	0.33	0.26	0.19	0.15	0.11
1-N-L	1.00	0.95	0.92	0.89	0.82	0.68	0.47	0.33	0.23	0.16	0.11	0.08	0.06
1-Y-SL	1.00	0.63	0.60	0.58	0.52	0.41	0.26	0.16	0.10	0.07	0.04	0.03	0.02
1-Y-SCL	1.00	0.63	0.60	0.58	0.51	0.40	0.24	0.15	0.09	0.06	0.04	0.02	0.01
1-Y-L	1.00	0.62	0.60	0.57	0.50	0.39	0.23	0.14	0.09	0.05	0.03	0.02	0.01
1-F-SL	1.00	0.98	0.97	0.96	0.93	0.88	0.78	0.70	0.63	0.56	0.50	0.44	0.40
1-F-SCL	1.00	0.96	0.94	0.93	0.87	0.77	0.61	0.48	0.38	0.30	0.23	0.18	0.14
1-F-L	1.00	0.96	0.93	0.91	0.83	0.71	0.51	0.37	0.27	0.19	0.14	0.10	0.07
2-N-SL	1.00	0.96	0.95	0.95	0.92	0.87	0.78	0.70	0.63	0.57	0.51	0.46	0.42
2-N-SCL	1.00	0.95	0.93	0.91	0.86	0.77	0.60	0.48	0.38	0.30	0.24	0.19	0.15
2-N-L	1.00	0.94	0.92	0.89	0.82	0.70	0.51	0.37	0.27	0.20	0.15	0.11	0.08
2-Y-SL	1.00	0.59	0.56	0.54	0.48	0.37	0.22	0.14	0.08	0.05	0.03	0.02	0.01
2-Y-SCL	1.00	0.59	0.56	0.53	0.46	0.35	0.20	0.12	0.07	0.04	0.03	0.02	0.01
2-Y-L	1.00	0.58	0.56	0.53	0.46	0.34	0.19	0.11	0.06	0.04	0.02	0.01	0.01
2-F-SL	1.00	0.96	0.95	0.94	0.92	0.88	0.80	0.73	0.67	0.61	0.56	0.51	0.46
2-F-SCL	1.00	0.95	0.93	0.92	0.87	0.78	0.64	0.52	0.42	0.34	0.28	0.22	0.18
2-F-L	1.00	0.94	0.92	0.90	0.84	0.74	0.57	0.44	0.34	0.26	0.21	0.16	0.13
3-N-SL	1.00	0.97	0.96	0.95	0.93	0.87	0.77	0.69	0.61	0.54	0.48	0.43	0.38
3-N-SCL	1.00	0.96	0.94	0.92	0.87	0.76	0.59	0.46	0.36	0.28	0.22	0.17	0.13
3-N-L	1.00	0.95	0.93	0.90	0.83	0.70	0.50	0.35	0.25	0.18	0.13	0.09	0.07
3-Y-SL	1.00	0.62	0.59	0.57	0.49	0.37	0.21	0.12	0.07	0.04	0.02	0.01	0.01
3-Y-SCL	1.00	0.62	0.59	0.56	0.48	0.36	0.20	0.11	0.06	0.03	0.02	0.01	0.01
3-Y-L	1.00	0.62	0.59	0.56	0.48	0.35	0.19	0.10	0.05	0.03	0.02	0.01	0.00
3-F-SL	1.00	0.97	0.96	0.95	0.93	0.88	0.79	0.71	0.64	0.57	0.51	0.46	0.41
3-F-SCL	1.00	0.96	0.95	0.93	0.88	0.78	0.62	0.50	0.39	0.31	0.25	0.20	0.16
3-F-L	1.00	0.96	0.93	0.91	0.84	0.71	0.52	0.38	0.28	0.20	0.15	0.11	0.08
4-N-SL	1.00	0.96	0.96	0.95	0.92	0.88	0.79	0.71	0.64	0.58	0.52	0.47	0.43

Scenario	0	1	2	3	6	12	24	36	48	60	72	84	96
4-N-SCL	1.00	0.95	0.94	0.92	0.87	0.78	0.63	0.50	0.40	0.32	0.26	0.21	0.17
4-N-L	1.00	0.95	0.92	0.90	0.83	0.71	0.53	0.39	0.29	0.22	0.17	0.13	0.10
4-Y-SL	1.00	0.61	0.59	0.56	0.48	0.36	0.20	0.12	0.07	0.04	0.02	0.01	0.01
4-Y-SCL	1.00	0.61	0.58	0.55	0.47	0.35	0.19	0.11	0.06	0.03	0.02	0.01	0.01
4-Y-L	1.00	0.61	0.58	0.55	0.47	0.34	0.18	0.10	0.05	0.03	0.02	0.01	0.00
4-F-SL	1.00	0.97	0.96	0.95	0.93	0.89	0.81	0.73	0.67	0.61	0.55	0.50	0.46
4-F-SCL	1.00	0.96	0.94	0.93	0.88	0.80	0.65	0.53	0.44	0.36	0.29	0.24	0.19
4-F-L	1.00	0.95	0.93	0.90	0.84	0.72	0.53	0.40	0.29	0.22	0.16	0.12	0.09
5-N-SL	1.00	0.94	0.93	0.92	0.90	0.86	0.78	0.71	0.64	0.58	0.53	0.48	0.44
5-N-SCL	1.00	0.93	0.91	0.90	0.85	0.77	0.62	0.51	0.41	0.34	0.28	0.23	0.19
5-N-L	1.00	0.92	0.90	0.88	0.82	0.71	0.53	0.41	0.31	0.24	0.19	0.15	0.12
5-Y-SL	1.00	0.52	0.50	0.47	0.40	0.30	0.16	0.09	0.05	0.03	0.02	0.01	0.01
5-Y-SCL	1.00	0.52	0.49	0.47	0.39	0.28	0.15	0.08	0.04	0.02	0.01	0.01	0.00
5-Y-L	1.00	0.52	0.49	0.46	0.39	0.27	0.14	0.07	0.04	0.02	0.01	0.01	0.00
5-F-SL	1.00	0.95	0.94	0.94	0.92	0.88	0.80	0.73	0.67	0.61	0.56	0.52	0.47
5-F-SCL	1.00	0.94	0.93	0.91	0.87	0.79	0.66	0.55	0.46	0.38	0.32	0.26	0.22
5-F-L	1.00	0.94	0.92	0.90	0.84	0.74	0.57	0.45	0.35	0.28	0.22	0.18	0.14
6-N-SL	1.00	0.93	0.93	0.92	0.90	0.86	0.78	0.71	0.65	0.59	0.54	0.50	0.46
6-N-SCL	1.00	0.93	0.91	0.89	0.85	0.77	0.63	0.52	0.43	0.36	0.30	0.25	0.21
6-N-L	1.00	0.92	0.90	0.87	0.82	0.71	0.54	0.42	0.33	0.27	0.21	0.17	0.14
6-Y-SL	1.00	0.52	0.49	0.47	0.40	0.29	0.16	0.09	0.05	0.03	0.02	0.01	0.01
6-Y-SCL	1.00	0.52	0.49	0.46	0.39	0.27	0.14	0.07	0.04	0.02	0.01	0.01	0.00
6-Y-L	1.00	0.52	0.48	0.46	0.38	0.26	0.13	0.07	0.03	0.02	0.01	0.01	0.00
6-F-SL	1.00	0.95	0.94	0.93	0.91	0.88	0.80	0.74	0.68	0.63	0.58	0.53	0.49
6-F-SCL	1.00	0.94	0.92	0.91	0.87	0.80	0.67	0.56	0.47	0.40	0.34	0.29	0.24
6-F-L	1.00	0.93	0.91	0.89	0.84	0.74	0.59	0.47	0.37	0.30	0.24	0.20	0.16
7-N-SL	1.00	0.94	0.94	0.93	0.91	0.87	0.80	0.74	0.68	0.63	0.58	0.53	0.49
7-N-SCL	1.00	0.94	0.92	0.91	0.87	0.80	0.67	0.57	0.48	0.40	0.34	0.29	0.24
7-N-L	1.00	0.92	0.90	0.89	0.84	0.76	0.63	0.51	0.42	0.34	0.28	0.23	0.19
7-Y-SL	1.00	0.50	0.47	0.45	0.37	0.26	0.13	0.07	0.03	0.02	0.01	0.00	0.00
7-Y-SCL	1.00	0.50	0.47	0.44	0.37	0.25	0.12	0.06	0.03	0.01	0.01	0.00	0.00
7-Y-L	1.00	0.50	0.47	0.44	0.36	0.25	0.11	0.05	0.03	0.01	0.01	0.00	0.00
7-F-SL	1.00	0.95	0.95	0.94	0.92	0.89	0.82	0.76	0.70	0.65	0.61	0.56	0.52
7-F-SCL	1.00	0.94	0.93	0.92	0.88	0.82	0.70	0.60	0.51	0.43	0.37	0.32	0.27
7-F-L	1.00	0.94	0.92	0.91	0.86	0.77	0.62	0.50	0.40	0.33	0.27	0.22	0.18
8-N-SL	1.00	0.94	0.93	0.93	0.91	0.87	0.80	0.74	0.68	0.63	0.58	0.54	0.50
8-N-SCL	1.00	0.93	0.92	0.91	0.87	0.80	0.68	0.58	0.49	0.42	0.36	0.31	0.26
8-N-L	1.00	0.93	0.91	0.89	0.84	0.75	0.60	0.48	0.39	0.32	0.26	0.22	0.18
8-Y-SL	1.00	0.50	0.47	0.44	0.37	0.26	0.13	0.06	0.03	0.02	0.01	0.00	0.00
8-Y-SCL	1.00	0.50	0.47	0.44	0.36	0.25	0.12	0.06	0.03	0.01	0.01	0.00	0.00
8-Y-L	1.00	0.50	0.47	0.44	0.36	0.24	0.11	0.05	0.02	0.01	0.01	0.00	0.00
8-F-SL	1.00	0.95	0.94	0.94	0.92	0.89	0.82	0.77	0.71	0.66	0.62	0.57	0.54
8-F-SCL	1.00	0.94	0.93	0.92	0.88	0.82	0.70	0.60	0.52	0.45	0.38	0.33	0.29
8-F-L	1.00	0.94	0.92	0.90	0.86	0.77	0.63	0.52	0.43	0.35	0.29	0.24	0.20

The numbers represent the pavement configuration; N = no edge drain; Y = clean edge drain; F = fouled edge drain; SL = silt loam; SCL = silty clay loam; L = loam